Center for Environmentally Sustainable Transportation in Cold Climates

Freeze-Thaw Durability and Long-Term Performance Evaluation of Shotcrete in Cold Regions

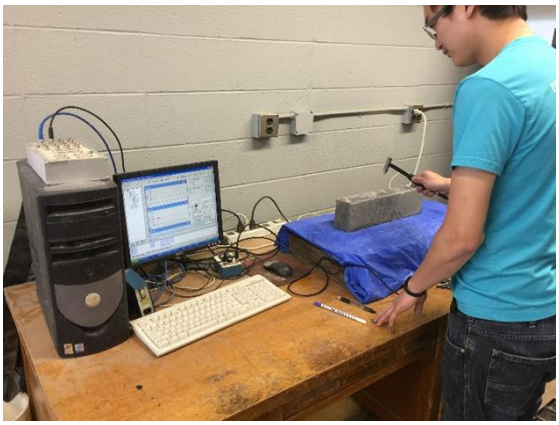

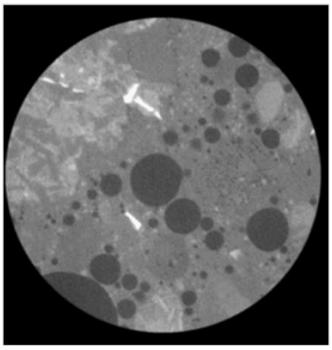

Pizhong Qiao, Ph.D., P.E., Professor
Zhidong Zhou, Graduate Research Assistant
Department of Civil and Environmental Engineering
Washington State University
Pullman, WA 99164-2910

Date: 12/31/2017

Prepared by: Pizhong Qiao and Zhidong Zhou

Center for Environmental Sustainable Transportation in Cold Climates
University of Alaska Fairbanks
Duckering Building, Room 245
P.O. Box 755900
Fairbanks, AK 99775

U.S. Department of Transportation
1200 New Jersey Avenue, SE
Washington, D.C. 20590

INE/AUTC 18.03

REPORT DOCUMENTATION PAGE

Form approved OMB No.

1. AGENCY USE ONLY (LEAVE BLANK)	2. REPORT DATE	3. REPORT TYPE AND DATES COVERED
	12/31/2017	Final Report: 11/2016 – 12/2017

4. TITLE AND SUBTITLE
Freeze-Thaw Durability and Long-Term Performance Evaluation of Shotcrete in Cold Regions

5. FUNDING NUMBERS

6. AUTHOR(S)
Pizhong Qiao, Ph.D., P.E., Professor
Zhidong Zhou, Graduate Research Assistant
Dept. of Civil & Environmental Engineering, Washington State University, Pullman, WA

7. PERFORMING ORGANIZATION NAME(S) AND ADDRESS(ES)
Center for Environmentally Sustainable Transportation in Cold Climates
University of Alaska Fairbanks
Duckering Building, Room 245
P.O. Box 755900
Fairbanks, AK 99775-5900

8. PERFORMING ORGANIZATION REPORT NUMBER

INE/AUTC 18.03

9. SPONSORING/MONITORING AGENCY NAME(S) AND ADDRESS(ES)
U.S. Department of Transportation
1200 New Jersey Avenue, SE
Washington, DC 20590

10. SPONSORING/MONITORING AGENCY REPORT NUMBER

11. SUPPLENMENTARY NOTES

12a. DISTRIBUTION / AVAILABILITY STATEMENT

No restrictions

12b. DISTRIBUTION CODE

13. ABSTRACT (Maximum 200 words)

This study's aim was to evaluate the freeze-thaw durability of shotcrete in cold regions and predict its long-term performance. One benchmark mix design from the WSDOT was chosen to prepare samples for performance evaluation. Shotcrete specimens were conditioned in accordance with ASTM C666. The long-term freeze-thaw performance after certain cycles was evaluated using the dynamic modulus of elasticity test (ASTM C215), fracture energy test (RILEM 50-FMC), and X-ray CT microstructure imaging analysis. Probabilistic damage analysis was conducted to establish the relation between the durability life and the damage parameter for different probabilities of reliability using the three-parameter Weibull distribution model. The fracture energy test was found to be a more sensitive test method than the dynamic modulus of elasticity for screening material deterioration over time and for capturing accumulative material damage caused by rapid freeze-thaw action, because of smaller durability factors (degradation ratios) obtained from the fracture energy test. X-ray CT imaging analysis is capable of detecting microcracks that form and pore evolution in the aggregate and interface transition zone of conditioned samples. Moreover, the continuum damage mechanic-based model shows potential in predicting long-term material degradation and the service life of shotcrete.

14- KEYWORDS : shotcrete; durability; freezing and thawing cyclic conditioning; dynamic modulus; fracture energy; X-ray CT; service life; Weibull model.

15. NUMBER OF PAGES
88

16. PRICE CODE
N/A

17. SECURITY CLASSIFICATION OF REPORT	18. SECURITY CLASSIFICATION OF THIS PAGE	19. SECURITY CLASSIFICATION OF ABSTRACT	20. LIMITATION OF ABSTRACT
Unclassified	Unclassified	Unclassified	N/A

Freeze-Thaw Durability and Long-Term Performance Evaluation of Shotcrete in Cold Regions

Final Report

Pizhong Qiao, Ph.D., P.E., Professor
Zhidong Zhou, Ph.D. Candidate and Graduate Research Assistant
Department of Civil and Environmental Engineering
Washington State University
Pullman, WA 99164-2910

Prepared by:

Pizhong Qiao and Zhidong Zhou

Prepared for

Center for Environmentally Sustainable
Transportation in Cold Climates
University of Alaska Fairbanks
Duckering Building, Room 245
P.O. Box 755900
Fairbanks, AK 99775

and

U.S. Department of Transportation
1200 New Jersey Avenue, SE
Washington, D.C. 20590

December 31, 2017

INE/AUTC 18.03

DISCLAIMER

This document is disseminated under the sponsorship of the U.S. Department of Transportation in the interest of information exchange. The U.S. Government assumes no liability for the use of the information contained in this document. The U.S. Government does not endorse products or manufacturers. Trademarks or manufacturers' names appear in this report only because they are considered essential to the objective of the document.

Opinions and conclusions expressed or implied in the report are those of the author(s). They are not necessarily those of the funding agencies.

METRIC (SI*) CONVERSION FACTORS

APPROXIMATE CONVERSIONS TO SI UNITS

Symbol	When You Know	Multiply By	To Find	Symbol
		LENGTH		
in	inches	25.4		mm
ft	feet	0.3048		m
yd	yards	0.914		m
mi	Miles (statute)	1.61		km
		AREA		
in^2	square inches	645.2	millimeters squared	cm^2
ft^2	square feet	0.0929	meters squared	m^2
yd^2	square yards	0.836	meters squared	m^2
mi^2	square miles	2.59	kilometers squared	km^2
ac	acres	0.4046	hectares	ha
		MASS (weight)		
oz	Ounces (avdp)	28.35	grams	g
lb	Pounds (avdp)	0.454	kilograms	kg
T	Short tons (2000 lb)	0.907	megagrams	mg
		VOLUME		
fl oz	fluid ounces (US)	29.57	milliliters	mL
gal	Gallons (liq)	3.785	liters	liters
ft^3	cubic feet	0.0283	meters cubed	m^3
yd^3	cubic yards	0.765	meters cubed	m^3

Note: Volumes greater than 1000 L shall be shown in m^3

		TEMPERATURE (exact)		
ºF	Fahrenheit temperature	5/9 (ºF-32)	Celsius temperature	ºC
		ILLUMINATION		
fc	Foot-candles	10.76	lux	lx
fl	foot-lamberts	3.426	candela/m^2	cd/cm^2
		FORCE and PRESSURE or STRESS		
lbf	pound-force	4.45	newtons	N
psi	pound-force per square inch	6.89	kilopascals	kPa

These factors conform to the requirement of FHWA Order 5190.1A *SI is the symbol for the International System of Measurements

APPROXIMATE CONVERSIONS FROM SI UNITS

Symbol	When You Know	Multiply By	To Find	Symbol
		LENGTH		
mm	millimeters	0.039	inches	in
m	meters	3.28	feet	ft
m	meters	1.09	yards	yd
km	kilometers	0.621	Miles (statute)	mi
		AREA		
mm^2	millimeters squared	0.0016	square inches	in^2 m^2
meters squared		10.764	square feet	ft^2 km^2
kilometers squared		0.39	square miles	mi^2 ha
hectares (10,000 m^2)		2.471	acres	ac
		MASS (weight)		
g	grams	0.0353	Ounces (avdp)	oz
kg	kilograms	2.205	Pounds (avdp)	lb mg
megagrams (1000 kg)		1.103	short tons	T
		VOLUME		
mL	milliliters	0.034	fluid ounces (US)	fl oz
liters	liters	0.264	Gallons (liq)	gal
m^3	meters cubed	35.315	cubic feet	ft^3
m^3	meters cubed	1.308	cubic yards	yd^3

		TEMPERATURE (exact)		
ºC	Celsius temperature	9/5 ºC+32	Fahrenheit temperature	ºF
		ILLUMINATION		
lx	lux	0.0929	foot-candles	fc
cd/cm ^{2}	candela/m^2	0.2919	foot-lamberts	fl
		FORCE and PRESSURE or STRESS		
N	newtons	0.225	pound-force	lbf
kPa	kilopascals	0.145	pound-force per square inch	psi

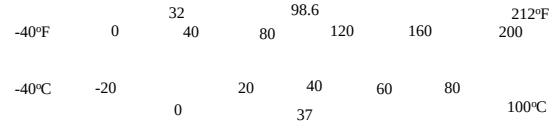

ACKNOWLEDGMENTS

The authors acknowledge the financial support provided by the Center for Environmentally Sustainable Transportation in Cold Climates (CESTiCC) and the Washington State Department of Transportation (WSDOT). The materials provided by the BASF Corporation and the nano-CT imaging analysis performed by Professor Lizhi Sun's group at the University of California Irvine (UCI) are gratefully acknowledged. The authors thank Mark Gaines, Marco Foster, Brain Aldrich, and Lu Sachao of WSDOT for their technical input and continuing support. The authors also appreciate the support and encouragement of Professor and Director Juanyu (Jenny) Liu of CESTiCC at the University of Alaska Fairbanks.

TABLE OF CONTENTS

LIST OF FIGURES

LIST OF TABLES

EXECUTIVE SUMMARY

The durability of shotcrete has been identified as an important performance aspect in best practices and quality assurance. One benchmark mix design from Washington State Department of Transportation was chosen to use in prepared test samples for performance evaluation, with emphasis on the long-term freeze-thaw resistance of shotcrete using dynamic modulus of elasticity and fracture energy tests. A probabilistic damage analysis was conducted to establish the relation between durability life and the damage parameter for different probabilities of reliability using the three-parameter Weibull distribution model.

The following findings are based on this extensive experimental study:

1. In measuring the dynamic modulus of elasticity and fracture energy of shotcrete after certain freeze-thaw conditioning cycles, the durability factors (relative values at 300 and 600 cycles) determined from fracture energy were found to be much smaller than those determined from dynamic modulus of elasticity, indicating that the fracture energy test is a more sensitive test method than the dynamic modulus of elasticity for screening material deterioration over time, and captures accumulative material damage subjected to rapid freeze-thaw action.

2. Porosity deterioration was observed under rapid freeze-thaw attacks through X-ray computed tomography imaging analysis. Some defects and cracks were also observed in the aggregate, cement matrix, and ITZ (interface transition zone) of conditioned samples. The deterioration speed of porosity increases with the number of freeze-thaw cycles because the formed defects and cracks provide more channels for moisture diffusion.

3. Based on the three-parameter Weibull distribution model, the relation between the degradation of dynamic modulus/fracture energy of shotcrete and the number of freeze-thaw cycles was established at different damage levels. As expected, the failure rate increases as

freeze-thaw cycles increase, indicating that shotcrete structures exhibit more potential risk of failure and less reliability as service life goes on and freeze-thaw attacks continue. The predicted results based on the polynomial probability model at 50% reliability are more consistent with the experimental results than at 90% reliability, which shows a more conservative and safer prediction.

The following observations and recommendations will improve the understanding of shotcrete and its long-term performance in cold climates:

1. "Before shooting" shotcrete specimens were prepared for evaluation and testing of their mechanical properties; however, they cannot be identical to specimens from "after shooting" shotcrete. The comparisons and correlations of the mechanical properties and durability of "before shooting" and "after shooting" types of shotcrete should be considered in a further study.

2. X-ray image analysis is capable of revealing the air-void system of shotcrete. The effects of air-void characteristics on the freeze-thaw durability of shotcrete need to be better understood, and eventually, the requirements of air content and spacing should be recommended for improved shotcrete application.

3. Only frost action was considered for the durability evaluation of shotcrete. However, since salty deicers are commonly used in cold regions to melt snow and ice and improve traffic safety, the resistance of shotcrete structures under more severe and combined frost and chemical attacks should be investigated. The corrosion effect of rebar on shotcrete performance in cold regions cannot be neglected.

4. Effective test methods are specifically needed for the evaluation and correlation of the field performance of shotcrete.

CHAPTER 1. INTRODUCTION

1.1 Problem Statement

In recent years, shotcrete has been used to replace cast-in-place (CIP) concrete as a structural earth-retaining component, such as fascia walls. Shotcrete has potential for use in traditional reinforced concrete retaining walls, if the economic benefits and good long-term performance of it in comparison with CIP concrete are demonstrated. Using shotcrete as a method of construction has become attractive in many states due to its potential for savings in cost and construction time. However, this practice could reduce the 75-year life expectancy of walls due to shotcrete's lack of homogeneous consolidation, inadequate air content, higher permeability, possible early rebar corrosion, premature failure of admixed synthetic fiber, etc. Further, shotcrete is prone to early drying shrinkage cracking and debonding from reinforcing bars or existing structures, compounding long-term durability concerns, especially in cold regions. Thus, there is a need to characterize shotcrete's long-term performance and durability.

This research aimed (1) to apply a promising and novel testing protocol (i.e., a cohesive fracture mechanics-based test method and a microstructural characterization approach combined with freezing, thawing, and accelerated weathering) for long-term shotcrete performance characterization; (2) to evaluate the damage accumulation and durability of shotcrete at cold temperatures with damage mechanics models; and (3) to recommend test methods for long-term performance characterization of shotcrete in cold regions. The outcomes of this study will benefit the construction and maintenance of transportation infrastructure in cold climates by exploring novel test methods for accelerated aging, evaluating and quantifying damage and durability, better understanding and predicting long-term performance and failure mechanisms of shotcrete

and its constituents in cold climates, and enhancing safety and security with better prediction of service life and longevity of retaining wall structures made of shotcrete.

1.2 Research Objectives

The goal of this project, in combination with related research work at Washington State Department of Transportation (WSDOT) (Qiao and Zhou 2017), was to evaluate and predict the degradation and durability of shotcrete in cold regions using accelerated conditioning and fracture tests and damage mechanics models. Our objectives were three-fold:

- To use a test protocol of micro (X-ray CT [computed tomography] scanning) and macro (cohesive fracture) test methods combined with accelerated freeze-thaw conditioning to characterize the long-term performance of shotcrete.
- To evaluate damage accumulation in shotcrete due to low temperature and freeze-thaw cycling using a phenomenological-based damage mechanics model and to understand the failure mechanisms and the potential for long-term deterioration of shotcrete.
- To develop recommendations for test methods on long-term performance characterization of shotcrete in cold regions.

CHAPTER 2. LITERATURE REVIEW

This chapter focuses on past studies related to characterizing and understanding the performance and durability of shotcrete, the advantages of using admixtures, and the effects of admixtures on the properties of shotcrete. Recent developments regarding the prediction models for freeze-thaw durability for concrete type of materials are reviewed.

2.1 Production and Mix of Shotcrete

2.1.1 Production

Shotcrete is regarded as a special construction technique for placing and compacting concrete rather than a special mixture design (Beaupre, 1994). Shotcrete is concrete that is conveyed through a pressurized hose to a nozzle at high velocity onto a receiving surface to form a structural or non-structural component of buildings; it is a process of simultaneous compaction, condensation, and hardening of concrete. Shotcrete is applied to surfaces using either a dry or wet mix method. The dry mix process contains a premixed blend of Portland cement and damp aggregate, which is pumped through the hose to the nozzle. Water is added from a separate hose in the nozzle and completely mixed with the dry mixture blend just as both streams are being sprayed onto the receiving surface (Figure 2.1a). The final quality of shotcrete is strongly affected by the experience of nozzleman (Crom, 1981). In wet mix concrete, all mix constituents are mixed with water and then pumped through a hose (Figure 2.1b). To achieve a high speed of pumping, additional compressed air is added in the nozzle. Compared with the dry mix process, the water of wet mix shotcrete is more accurately controlled by delivery equipment, and the wet mix shotcrete is applied at a much higher production rate. Some finishes can be subsequently applied to fresh shotcrete structures; for example, a thin surface coating component can be

directly sprayed onto the surface to avoid internal moisture loss.

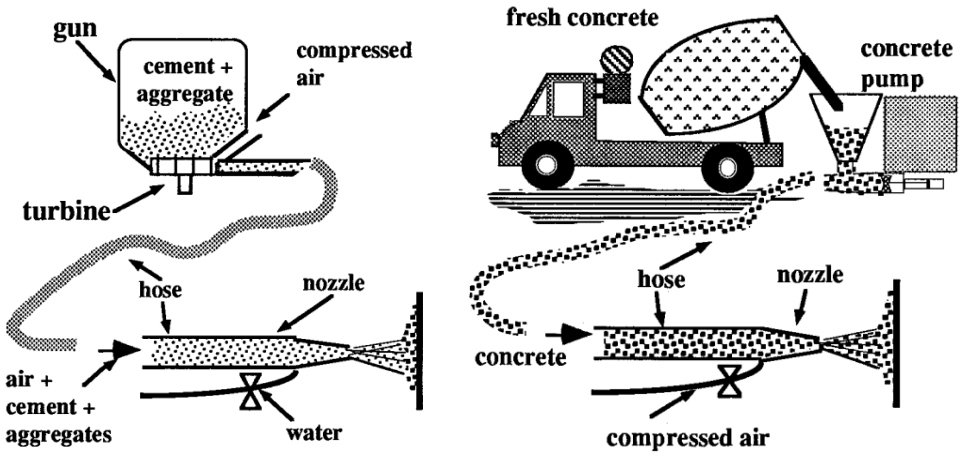

(a) (b)

Figure 2.1 Schematic of shotcrete production: (a) dry-mix process; and (b) wet-mix process (Beaupre, 1994)

2.1.2 Mix constituents

The mix constituents of normal concrete are primarily Portland cement, aggregates, and water. However, other ingredients are added to improve the mechanical properties, workability, and pumpability of shotcrete in some applications. These ingredients include silica fume, ground granulated blast-furnace slag (GGBFS), air-entraining admixtures, water-reducing admixtures, accelerators, and fibers.

The water/cement ratio of shotcrete depends on field application, but generally varies from 0.3 to 0.6. A typical wet mix design for shotcrete is shown in Table 2.1 (Jolin and Beaupre, 2003). A relatively lower water/cement ratio is required in production of high performance shotcrete. Normal types of cement, river sand, and coarse aggregate can be used to produce shotcrete. The nominal maximum aggregate size is usually 3/4 inch or smaller. The ACI Committee 506 (2005) has recommended grading limits for shotcrete to minimize drying shrinkage and rebound (Table 2.2). Shotcrete produced with finer aggregates exhibits greater

drying shrinkage, while shotcrete produced with coarser aggregate results in more rebound.

Table 2.1 Typical wet-mix shotcrete composition (Jolin and Beaupre, 2003)

Material	Quantity for 1 m^3
Portland Cement	400 kg (880 lb)
Silica Fume	40 kg (88 lb)
Fine Sand	1110 kg (2447 lb)
Coarse Aggregate (max 10 mm [3/8 in.])	460 kg (1014 lb)
Water	180 kg (396 lb)
Water-Reducing Admixture	1500 ml (51 fl oz.)
Superplasticizer	5000 ml (170 fl oz.)
Air-Entraining Admixture	2500 ml (84 fl oz.)
w/c	0.41

Table 2.2 Grading limits for aggregate of shotcrete (ACI 506)

Sieve Size	Percent by Mass Passing Individual Sieves		
	Grading No. 1	Grading No. 2	Grading No. 3
3/4 in.	-	-	100
1/2 in.	-	100	80-95
3/8 in.	100	90-100	70-90
No. 4	95-100	70-85	50-70-
No. 8	80-100	50-70	35-55
No. 16	50-85	35-55	20-40
No. 30	25-60	20-35	10-30
No. 50	10-30	8-20	5-17
No. 100	2-10	2-10	2-10

Silica fume, a waste byproduct of the silicon metal and alloy production process, has been widely utilized to improve the strength, durability, and sustainability of concrete and shotcrete (Morgan and Wolsiefer, 1992; Zhang et al., 1999; Sawoszczuk et al., 2013).

Replacement ranges from 7% to 15% by mass of cement (U.S. Army Corps of Engineers, 1993).

GGBFS, a waste byproduct of the iron production process, has been widely utilized to achieve a certain performance of shotcrete, including slower setting time, lower heat generation during hydration, and higher chloride-ion resistance (Sawoszczuk et al., 2013). Thus, the addition of GGBFS may exhibit some interaction issues with the use of accelerators.

Air-entraining admixtures are essential to improving the pumpability and freeze-thaw durability of shotcrete. Small air bubbles are initially created during mixing, and most of the bubbles are lost during pumping and shooting. Therefore, the recommended air content of fresh shotcrete after mixing is higher than 12% to compensate for these losses (Morgan, 2003).

Water-reducing admixtures are important to improve the workability of shotcrete, especially for high performance shotcrete, to allow the lower water-cement ratio to be used.

Accelerators (accelerating admixtures) are used extensively in shotcrete when rapid section buildup and early strength development are required, such as in tunnel construction. However, accelerators may decline due to increasing use of silica fume (Prudencio, 1998).

Fibers in shotcrete have been used to enhance its ductility, toughness, and fatigue resistance and reduce crack propagation (Verma, 2015).

2.2 Properties of Shotcrete

2.2.1 Air content and mechanical properties

The pumpability and shootability of fresh wet-mix shotcrete are important rheological parameters, and they can be determined by slump and air content tests (Yun et al., 2015a; 2015b). The related air-void system is an essential parameter that affects the mechanical properties and freeze-thaw durability of shotcrete (Morgan, 2003; Fonseca and Scherer, 2015; Choi et al., 2016). The ingredients used in shotcrete can have a significant effect on air content. The

pumpability and shootability of fresh shotcrete can be achieved by adjusting the amounts of water-reducing admixtures and air-entraining admixtures from an optimal mix design test. It is usually considered that slump of 4–8 inches and air content of 10–20% are acceptable. The air content of hardened shotcrete is excessively affected by production procedures, construction practices, and weather, such as the method of batching, time and speed of mixing, transportation and delivery, pumping and shooting, and temperature (Portland Cement Association, 1998; Choi, 2008; Zhang, 2012).

There are no specific testing methods for fresh or hardened shotcrete. All tests considered for conventional concrete are applicable to shotcrete. Similar to conventional concrete, the properties of shotcrete are mainly controlled by mixture design parameters, i.e., water/cement ratio, content and type of cement, size and type of aggregate, admixtures used, energy and duration of mixing process, and curing conditions (U.S. Army Corps of Engineers, 1993). The proper use of silica fume, GGBFS, accelerators, and fibers can significantly improve certain properties of shotcrete. In addition, the shooting method used (dry or wet mix) influences its properties. The higher the air content of shotcrete after shooting, the lower strength it achieves.

Compressive strength ranging from 4,000 psi (27.5 MPa) to 10,000 psi (68.9 MPa) at 28 days has been reported in field construction (Zhang, 2014). The early age strength of shotcrete can be higher than conventional concrete, reaching 1,000 psi in 5 hours and 3,000 psi in 24 hours (Heere and Morgan, 2002). The strength of shotcrete tends to increase with decreased air content and a decreased spacing factor, when compared with the same mixture without shooting. Shotcrete after shooting exhibits a 6–10% loss of air content and a 20–70% increase in strength (Choi et al., 2016). The addition of silica fume and GGBFS usually improves mechanical properties and durability, since they improve bond strength between cement paste and

aggregates. Won et al. (2013) found that the addition of mineral-based accelerator increased early age strength, while some test samples exhibited better long-term strength. Banthia et al. (1994), Zhang et al. (1999), and Verma (2015) showed that the use of fibers in shotcrete significantly improved ductility and flexural strength, and slightly improved compressive strength. Accelerators are commonly used to increase early strength and achieve rapid set (Prudencio 1998). A hot environment may benefit strength growth and subsequent integrity at early age (Lee et al., 2013).

Considering that shotcrete is sprayed on existing structures (hard rock, slopes, rebar, etc.) as a support system, the adhesion strength between shotcrete and the existing structure is one critical property of shotcrete. Bryne et al. (2014a; 2014b) developed a pull-out test method to evaluate early age adhesion strength several hours after shooting. At a very early time after spraying, the physical properties and adhesion strength depend on the set accelerator and the formed microstructure. The failure location of the shotcrete layer is another aspect to be considered. Malmgren et al. (2005) observed that failure was more likely to occur where the shotcrete layer is thinner than or equal to 20 mm and with a low adhesion strength. Karlsson (1980) found from a field study that among only 32% of 238 tests, the whole failure occurred at the contact area. Malmgren et al. (2005) found from the restrained shrinkage tests that relatively fewer cracks occurred at the contact between shotcrete and substrates, which indicates that restrained shrinkage could destroy the bond between shotcrete and substrates. The type of surface preparation also has significant influence on the long-term bond strength of shotcrete (Talbot et al., 1995). Improvement of the adhesion strength showed a reliable relation with the growth of compressive strength.

2.2.2 Durability performance

Shotcrete infrastructures located in cold climates frequently suffer from freeze-thaw cycles as well as deicer salt attack during winter seasons. Both frost damage and salt scaling can reduce strength and the modulus of elasticity and eventually lead to structural damage or loss in serviceability. Many studies have been conducted on the durability of shotcrete (Beaupre et al., 1994; Lamontagne et al., 1996; Jolin et al., 1997; Morgan, 2003; Mainali et al., 2015; Wang et al., 2015a; Wang et al., 2015b). The resistance of shotcrete to freeze-thaw action can be determined in accordance with ASTM C 666 (2015), and the air content of fresh shotcrete and the air content and spacing factor of hardened shotcrete specimens can be determined following ASTM C231 (2014) and ASTM C 457 (2012), respectively. Some other methods were adopted to study the pore structures and permeability of shotcrete, such as X-ray diffraction, acoustic emissions (AE), thermogravimetry-differential scanning calorimetry (TGA-DSC), and scanning electron microscopy (SEM). A typical damage process of shotcrete after suffering sulfate attack and drying-wetting cycles is shown in Figure 2.1. Since the use of shooting technology, some differences of internal structure and durability have been shown between shotcrete and ordinary concrete (Niu et al., 2015; Jiang et al., 2015).

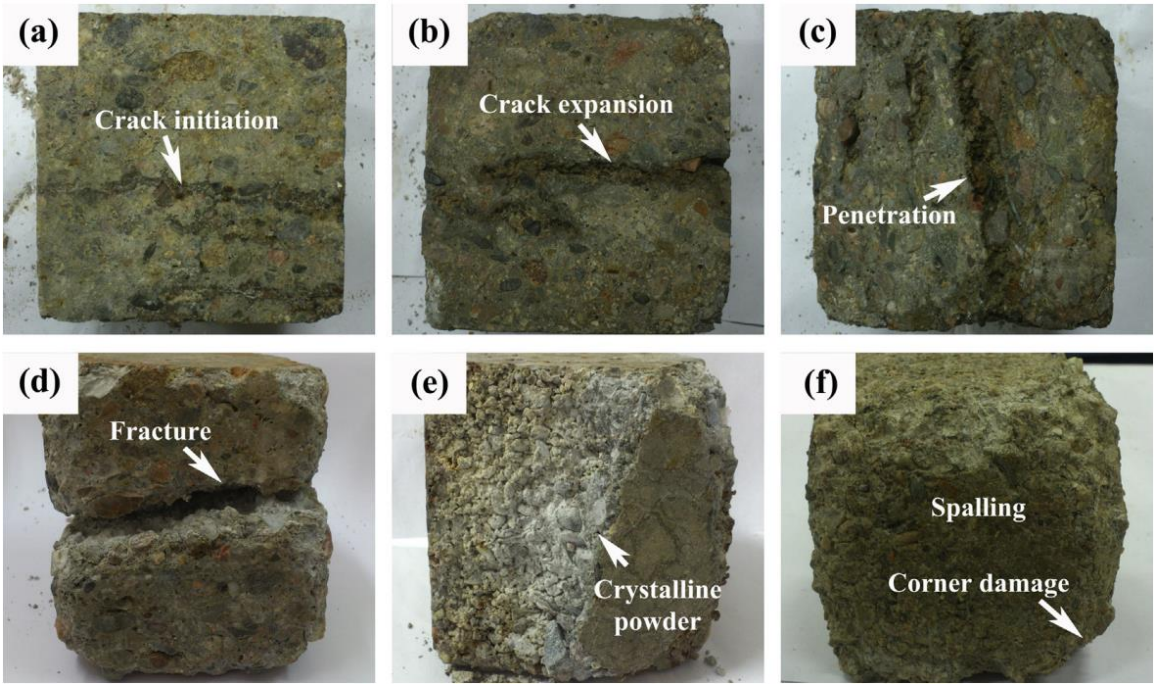

Figure 2.2 Appearances of damage process after suffering sulfate attack and drying-wetting cycles: (a) shotcrete, 30 days; (b) shotcrete, 60 days; (c) shotcrete, 90 days; (d) and (e) shotcrete, 140 days; and (f) ordinary concrete, 140 days. (Niu et al., 2015)

The internal air-void system of hardened shotcrete has significant influences on the durability of shotcrete (Choi et al., 2016). Air-entraining admixtures are important to ensure freeze-thaw and deicer salt scaling resistance (Lamontagne et al., 1996; Chen et al., 2015). The deicer salt scaling resistance of both dry and wet mix shotcrete is improved with increased air content and decreased spacing factor, and use of silica fume generally reduces the mass of scaling residue and improves the durability of shotcrete (Morgan and Wolsiefer, 1992; Beaupre et al., 1994; Choi. et al., 2016). Some accelerators improve the durability of shotcrete due to its excellent strength, permeability, and freeze-thaw cycle resistance (Park et al., 2008).

2.2.3 Effects of admixtures

Yun et al. (2015b) studied the effects of various admixtures on the rheological properties of high-performance wet-mix shotcrete (HPWMS), e.g., silica fume, air-entraining admixtures,

superplasticizer, synthetic fiber, powdered polymer, etc. The yield stress and plastic viscosity of HPWMS with various types and amounts of admixtures were measured using an IBB rheometer to determine pumpability and shootability. The air-entraining agent tended to proportionally reduce both the flow resistance and torque viscosity of HPWMS. Superplasticizers showed relatively greater influence on flow resistance than torque viscosity. Silica fume increased flow resistance while slightly reducing torque viscosity. Silica fume greatly improved the shootability and pumpability of shotcrete.

Park et al. (2008), Won et al. (2013), and Won et al. (2015) compared the mechanical properties of shotcrete containing different contents of high-strength cement-based mineral (HS-CM) accelerator with shotcrete containing 5% of normal cement-based mineral accelerator (CM). They found that shotcrete containing more than 6% HS-CM with respect to cement weight was slower at initial set, but faster at final set than that made with CM. HS-CM accelerated shotcrete had approximately the same compressive and flexural strength at early age, but had higher compressive and flexural strength at 7 days and 28 days than CM accelerated shotcrete. Based on microstructural analysis using scanning electron microscope (SEM), X-ray diffraction (XRD), and nitrogen adsorption tests, these researchers also found that shotcrete made with HS-CM showed better frost and chemical resistance than shotcrete made with CM. The alkali-silica reaction of accelerating admixtures in shotcrete is another phenomenon being investigated. Length change of cement pastes made with various accelerating admixtures under sulfate solution was measured to characterize the expansion caused by alkali-silica reaction. Paglia et al. (2003) observed that accelerated cement pastes showed more expansion up to 6 months than unaccelerated cement pastes. Won et al. (2012) showed that the expansion of accelerated shotcrete increased with the total equivalent alkali content of the specimens.

2.3 Prediction Models for Freeze-Thaw Durability

ASTM C666 with its accelerated freezing and thawing test method is commonly used for durability evaluation, during which the dynamic modulus of elasticity is measured in a nondestructive approach, and other material properties are not frequently adopted for comparison. Some models have been proposed to explore the relation between degradation of material and accelerated freezing and thawing testing cycles.

2.3.1 Empirical models

The frost resistance of concrete/shotcrete can be solely expressed by the reduction of dynamic modulus of elasticity of concrete and the number of freeze-thaw cycles (Chen and Qiao, 2015). It is more reasonable, however, to formulate the relationship by involving some affecting factors, because reduction of the dynamic modulus of elasticity can show some relation with the AEA content, porosity, density, water-cement ratio, type and content of cementitious materials, etc. Based on a large number of experiments related to air-void characterization and reduction of dynamic modulus of elasticity, and/or other material properties (such as, strength), such relationships can be formulated using regression analysis (Fujiwara, 1987; Kim et al., 2013; Wang et al., 2015a). However, these prediction formulas for frost resistance of concrete were composed experientially and empirically based on testing results, and they could not reveal fundamental aspects of frost mechanisms in consideration with the actual natural environment.

2.3.2 Mathematical and theoretical models

It has been stated that moisture transport is the key factor in deterioration of concrete (Setzer et al., 1997). Powers and Helmuth (1953) assumed that frost damage of concrete was caused by hydrostatic pressure induced by expulsion and freezing of water, which is a pure physical process. Concrete is subjected to unloading during the thawing process. Helmuth (1960)

later extended and modified the hydraulic pressure theory to the osmotic pressure theory by considering capillary porosity. Bazant et al. (1988) proposed a comprehensive mathematical model that mainly focused on the deterministic nature of the process involved in freezing and thawing of concrete. Bazant et al.'s (1988) model formulated the diffusion of water, heat conduction, and stress superposition within concrete. In addition, Bazant et al. (1988) considered the effects of pore size distribution, permeability, and size and shape of cross-sections. However, they pointed out that it was very complicated to apply such a complex mathematical model, because various new tests were required to determine model parameters, though finite-element analysis might provide a feasible approach.

2.3.3 Probabilistic damage models

Cyclic freezing and thawing damage of concrete can be recognized as low-cycle fatigue damage accumulation due to internal hydrostatic and osmotic pressure. Analogously, fatigue damage models can predict cyclic frost damage behavior in cementitious materials. Similar to other important degradation mechanisms considered in concrete structures (such as corrosion of rebar, carbonation, etc.), the freezing and thawing damage accumulation of cementitious materials also exhibits stochastic behavior with a specific distribution (Shen et al., 2000). It is feasible to use probabilistic damage models to investigate deterioration mechanisms in concrete structures as well as predict structural reliability (Sudret, 2008). Focused on the deterioration of concrete due to long-term freezing and thawing action, researchers successfully established the relationship between number of freeze-thaw cycles and damage parameters at different probabilities of reliability using a combined Weibull distribution and probabilistic damage model (Chen and Qiao, 2015; Qiao and Chen, 2013). In these studies, the reductions of dynamic modulus of elasticity and fracture energy were adopted to characterize the deterioration of concrete.

In summary, studies on analytical and empirical models to predict the durability and long-term performance of concrete are very limited. No prediction models of durability and aging of shotcrete were found.

CHAPTER 3. MATERIALS AND EXPERIMENTAL PROGRAM

In this chapter, combined with a related study by WSDOT (Qiao and Zhou 2017), the materials and experimental testing programs to evaluate fresh and hardened properties of shotcrete, including flowability, compressive and tensile strength, modulus of elasticity, and durability assessment, are presented.

3.1 Materials and Mix Design

The cementitious materials, including Portland cement Type I-II, silica fume (SF), and ground granulated blast-furnace slag (GGBFS), were provided by Lafarge NA-PNW District. Coarse aggregate and fine sand were provided by Pre-Mix, Inc., a local concrete company in Pullman, WA. The nominal maximum size of coarse aggregate used in this study was 3/8 inch. The grain size distribution of coarse aggregate and fine sand from sieve analysis in accordance with ASTM C136 (2014) are presented in Table 3.1. The coarse aggregate and fine sand for shotcrete met the requirements of AASHTO #8 and WSDOT Class 2 Sand. The corresponding specific gravity and water absorption were determined in accordance with ASTM C127 (2015) and ASTM C128 (2015), respectively; their values are given in Table 3.1.

Table 3.1 Grain size distribution of aggregates (sieve analysis)

Type	Shotcrete, Cumulative % Passing	
Sieve Size	Coarse Aggregate	Fine Aggregate
1/2	100	--
3/8"	99.1	100.0
1/4"	37.3	99.5
#4	6.9	85.7
#8	3.2	58.5
#16	1.8	35.6
#30	1.2	16.0
#50	0.9	4.8
#100	0.8	2.1
#200	--	--
Specific Gravity	2.69	2.64
Absorption Capacity, %	1.21	1.89

Two types of commercially available chemical admixtures were used to produce shotcrete: air-entraining admixture (AEA) and high-range water reducing admixture (HRWRA); both are produced by BASF Construction Chemicals, LLC. Grace Construction Products provided 1000 air-entraining admixture, which was used to produce proper air content in the concrete mixes. Glenium 3030 NS, a polycarboxylate-based HRWRA, was used to achieve desired workability and pumpability. The volume contents of AEA and HRWRA for shotcrete were determined based on the measurements made on the fresh mixed shotcrete in the trial mix design tests.

One mix design considered for the shotcrete batch is summarized in Table 3.2, along with the benchmark mix design of shotcrete from the WSDOT (see Appendix A).

Table 3.2 WSDOT mix design

Mixture	Cement (lb/yd^3)	Silica Fume (lb/yd^3)	GGBFS (lb/yd^3)	Coarse (lb/yd^3)	Sand (lb/yd^3)	w/cm	Water (lb)
Shotcrete	705	50	40	2120	790	0.34	267

3.2 Sample Preparations

Pumping and shooting are two basic operation procedures in shotcrete construction, whenever wet-mix shotcrete or dry-mix shotcrete is used. In previous studies, evaluation of shotcrete usually regards two terms: “before shooting” and “after shooting,” also known as “without shooting” and “with shooting.” Since the goal of this study was to investigate the long-term freeze-thaw durability performance of shotcrete in cold regions, the effect of pumping and shooting was not considered. Thus, only “before shooting” shotcrete was studied.

The mixing of constituents to produce shotcrete specimens was performed at the concrete laboratory of Washington State University by a concrete drum mixer with a volume of 3.5 cubic feet. The mixing procedures were as follows:

1. All the materials were batched by weight.

2. Two pounds of water and two pounds of cement were mixed together and used to wet inside the drum of the concrete mixer. Then, the paste was dumped.

3. All pre-weighted aggregates and sand were added in the mixer and mixed for 1/2 minute.

4. All the pre-weighted cementitious materials (cement, silica fume, and/or GGBFS) were added in the mixer. The air-entraining admixture (AEA) was added to half of the water, and the water solution was then added in the mixer. They were mixed for 3 minutes.

5. The rest of the water was added, and they were mixed for 2 minutes.

6. High range water reducing admixture (HRWRA) and SRA were added separately, and they were mixed for 3 minutes.

7. The mix rested for 2 minutes.

8. The mix was mixed for the final 2 minutes.

9. The slump test was conducted first.

10. The air content test was then conducted.

11. Necessary adjustments of HRWRA and AEA were made until the targeted slump and air content were achieved.

As soon as mixing was completed, the fresh shotcrete was poured into oiled wooden/steel molds to cast specimens in accordance with ASTM C192 (2016). Specimens were externally vibrated for approximately 10 seconds using a vibrating table. The curing of all specimens consisted of two phases: initial curing after casting and standard curing prior to testing. All specimens in the molds were initially cured in a vibration-free fog room with a temperature of 73.5 ± 3.5°F (23.0 ± 2.0°C) from the time of casting. After approximately 24 hours, specimens were demolded, and the standard curing period began. Specimens for mechanical tests were soaked in lime-saturated water storage tanks in a curing room with a temperature of 73 ± 3°F (23 ± 2°C) until testing age.

3.3 Experimental Testing Program

A series of tests was conducted to evaluate the properties of shotcrete in fresh and hardened states. Slump and air content were tested to evaluate the workability and pumpability of fresh shotcrete and ensure the durability of hardened shotcrete. Similar to the test methods used with hardened concrete, the hardened shotcrete property tests include two categories: Category 1 is related to the mechanical properties of shotcrete at different ages, such as

compressive strength, flexural strength, modulus of elasticity, etc. Category 2 is related to the long-term durability evaluation of shotcrete under rapid freeze-thaw action, and corresponding tests include dynamic modulus of elasticity, cohesive fracture, and X-ray CT scanning to characterize degradation of material properties after different numbers of freeze-thaw cycles. The procedures for each test in these two categories are briefly discussed in the following sections. The tests considered in this study are summarized in Table 3.3; their corresponding ASTM/AASHTO standard test method designations are included. For all tests, at least three replicates were tested.

Table 3.3 Experimental testing program

Properties	Test Methods	Condition
Fresh Properties of Shotcrete		
Slump	ASTM C143	Fresh
Air content	ASTM C231	Fresh
Unit Weight	ASTM C138	Fresh
Hardened Properties of Shotcrete		
Compressive Strength	ASTM C39	6″×12″ cylinder @ 7, 14, and 28 days
Flexural Strength	ASTM C78	3″×4″×16″ prism @ 7, 14, and 28 days
Modulus of Elasticity	ASTM C469	6″×12″ cylinder @ 7, 14, and 28 days
Freezing-Thaw Dynamic Modulus Fracture Energy	ASTM C666 ASTM C215 RILEM 50-FMC	3″×4″×16″ prism Begins after initial curing of 28days; @ 0, 60, 120, 180, 240, 300, 450, and 600 cycles
X-ray CT scanning	---	@ 0, 300, and 600 cycles

3.3.1 Properties of fresh shotcrete

The slump test (Figure 3.1) was performed following the procedures of ASTM C143 (2015) "Standard Test Method for Slump of Hydraulic Cement Concrete." Based on the pressure method, a Type-B Air Meter was used to measure air content, which follows ASTM C231 "Standard Test Method for Air Content of Freshly-Mixed Concrete by the Pressure Method" (Figure 3.2). In the meantime, the unit weight of fresh shotcrete was determined following the procedures of ASTM C138 (2016) "Standard Test Method for Density (Unit Weight), Yield, and Air Content (Gravimetric) of Concrete." Pumpability and shootability of fresh wet-mix shotcrete are important rheological parameters for construction practices (Yun et al., 2015a; 2015b). Air content of fresh wet-mix shotcrete is also critical for improving the air-void system and freeze-thaw durability of shotcrete (Morgan, 2003; Fonseca et al., 2015; Choi et al., 2016). After transportation and delivery, pumping, and shooting, the air content of in-place shotcrete will decrease considerably (U.S. Army Corps of Engineers, 1993; Choi, et al., 2016). Slump of 4 in. to 8 in. and air content of 8–20% is acceptable for fresh shotcrete. Thus, the amounts of HRWRA and AEA are adjusted to achieve a slump target (i.e., 5 inch) and a target air content (i.e., 10%).

Figure 3.1 Slump test

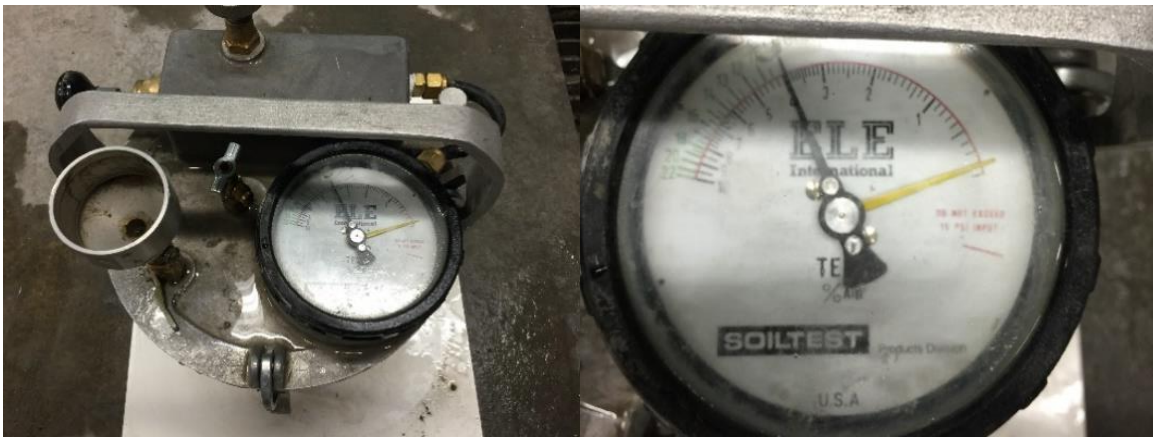

Figure 3.2 Air content test by pressure method

3.3.2 Mechanical properties of hardened shotcrete

Three basic mechanical properties of hardened shotcrete/CIP concrete—compressive strength, modulus of elasticity, and flexural strength—were evaluated at different ages.

The compressive strength test was conducted on 6 inch × 12 inch cylinders following the procedures of ASTM C39 (2016) "Standard Test Method for Compressive Strength of Cylindrical Concrete Specimens" (Figure 3.3). The compressive test was conducted at a specific stress rate of 35 ± 7 psi/s. Therefore, the required loading rate was calculated corresponding to the size of the specimen, i.e., 60000 ± 12000 lbf/min.

The modulus of elasticity test was conducted following the procedures of ASTM C469 (2014) "Standard Test Method for Static Modulus of Elasticity and Poisson's Ratio of Concrete in Compression" (Figure 3.4). The load was applied corresponding to a specific stress rate of 35 ± 7 psi/s, until it reached 40% of the average ultimate load of the 6 inch × 12 inch cylindrical specimens.

The flexural strength test was performed in accordance with ASTM C78 (2016) "Standard Method of Test for Flexural Strength of Concrete (Using Simple Beam with Third-Point Loading)" (Figure 3.5). A constant loading rate was applied at a specific tensile stress rate

within the range of 125 to 175 psi/min, i.e., 5,000 to 7,000 lbf/min for the 3 inch × 4 inch × 16 inch prisms.

Figure 3.3 Compressive strength test

Figure 3.4 Modulus of elasticity test

Figure 3.5 Flexural strength test (3 inch × 4 inch × 16 inch prism, span: 12 inch)

3.3.3 Freeze-thaw durability evaluation

In addition to standard test protocol (e.g., ASTM C215 [2014]), other methods were used to evaluate the frost resistance of shotcrete, including the use of fracture energy analysis and X-ray CT imaging. Shotcrete specimens were subjected to accelerated freeze-thaw conditioning and measured with the hammer impact test (i.e., dynamic modulus). In parallel, the X-ray CT images of the shotcrete samples at different defined freeze-thaw cycles were accordingly obtained. Fracture energy tests were also conducted on prismatic specimens with certain freeze-thaw conditioning cycles to characterize durability of the specimens in terms of fracture strength and fracture energy.

3.3.3.1 Rapid freeze and thaw test

The manufactured UHPC prism samples were conditioned using the rapid freeze-thaw test in accordance with ASTM C666 Procedure A (2015), which is designed to evaluate the potential frost resistance of concrete in cold climates. The temperature range of 0° to 40°F was considered in the freeze-thaw cycles, and the cycle frequency was about six freeze-thaw cycles per day. The condition chamber used is shown in Figure 3.6. For the dynamic modulus tests, three samples with dimensions of 3 inch × 4 inch × 16 inch were conditioned in the chamber as the “conditioned group,” and another three were soaked in water as the “control group” for comparison. More than 24 specimens were cast from the same batch and conditioned in the chamber for fracture energy and X-ray CT imaging analysis.

Figure 3.6 Freeze-thaw conditioning machine

3.3.3.2 Dynamic modulus test

The dynamic modulus of elasticity of prismatic concrete samples was obtained every 30 freeze-thaw cycles using the transverse frequency test in accordance with ASTM C215 (2014). The dynamic modulus of shotcrete prism samples under different freeze-thaw conditioning cycles at every 30 cycles was evaluated using the transverse frequency test. The dynamic modulus test is an impact test method that measures transverse frequency using either an accelerometer or a piezoelectric sensor attached to one end of the beam. The relative dynamic modulus is then computed using the fundamental transverse frequencies at 0 cycle or after a certain number of freeze-thaw cycles. The test setup for dynamic modulus of elasticity measurement is shown in Figure 3.7. Data reduction procedures are explained in detail in Qiao et al. (2012). The dynamic modulus of shotcrete beam samples at different cycles (up to 600 freeze-thaw cycles) was compiled. A decrease of the dynamic modulus over accelerated freeze-thaw cyclic conditioning indicates degradation of concrete materials.

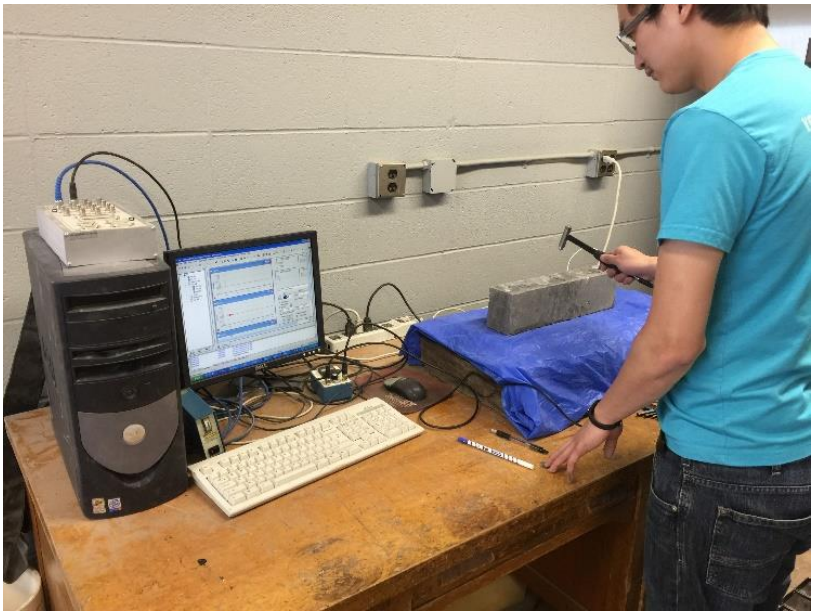

Figure 3.7 Dynamic modulus test setup at WSU

The dynamic modulus of elasticity, *E* (in Pascal [Pa]), can be determined from the fundamental transverse frequency, mass, and dimensions of the test sample. The equation is defined as:

$$E = CMn^2 \tag{3.1}$$

where *M* is the mass of the sample;

n is the fundamental transverse frequency;

C=0.9464$T\frac{L^3}{bt^3}$ for a prism;

L is the length of the sample;

t and *b* are the thickness and width of the sample, respectively;

T is a correction factor (= 1.41 in this study) that depends on the ratio of the radius of gyration to the length of the specimen and the Poisson's ratio.

The dynamic modulus of elasticity values of the concrete samples at different cycles was compiled and compared. The relative dynamic modulus of elasticity was calculated as the ratio

of initial dynamic modulus at 0 cycle to that at a certain number of freeze-thaw cycles. The decrease of the dynamic modulus of elasticity over accelerated freeze-thaw cyclic conditioning indicates the degradation of concrete materials. Continuation of testing samples after their relative dynamic modulus of elasticity has fallen below 60% is not recommended.

3.3.3.3 Cohesive fracture test

The cohesive fracture test was conducted to evaluate the fracture energy of shotcrete samples at different freeze-thaw cycles. Fracture energy is a material property that is as important as normal strength or modulus properties; it is considered to characterize material degradation under rapid freeze-thaw attacks (Chen and Qiao, 2015). In accordance with the RILEM TC-50 FMC (1985), the evaluation of fracture energy was performed based on a notched three-point bending beam with dimensions of 3 inch × 4 inch × 16 inch, as shown in Figure 3.8. The depth of the notch was fabricated as half the depth of the specimen using a diamond saw. More related information can be found in Qiao and Chen (2013).

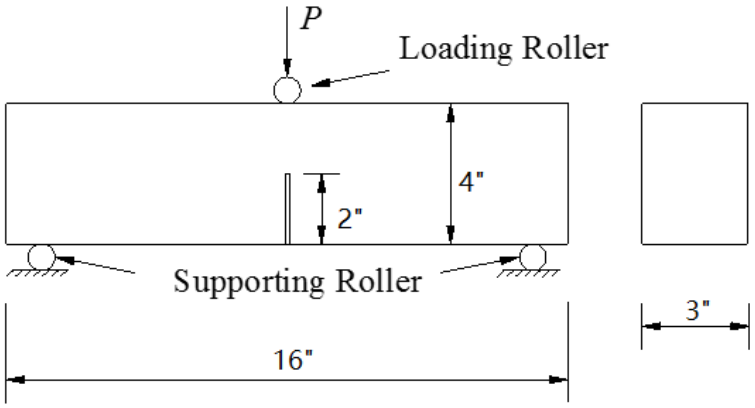

Figure 3.8 Sketch diagram of cohesive fracture test under three-point bending

All fracture tests were performed on an MTS servo-hydraulic testing machine using the test setup shown in Figure 3.9. The tests were conducted under displacement-controlled mode, i.e., at a loading rate of 0.0236 in./min. Two Linear Variable Differential Transducers (LVDT)

oppositely mounted on the specimen were used to measure the mid-span deflection (MSD) (δ) of the specimen. Both loading and mid-span deflection were recorded simultaneously by the machine.

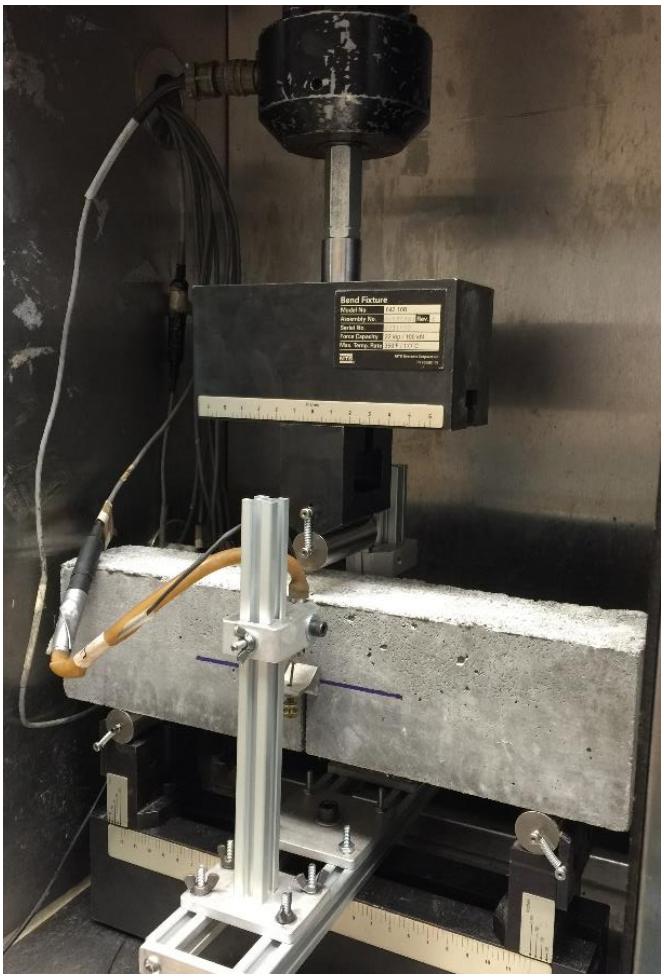

Figure 3.9 Testing equipment setup for fracture test

A typical load-deflection (*P*-*δ*) curve obtained from a cohesive fracture test is illustrated in Figure 3.10, in which *P* is the measured load and δ is the average mid-span deflection of two LVDTs. The additional load P_1 is the self-weight of the specimen. Accordingly, the total work energy *W* can be calculated using Equation 3.2.

$$W = W_0 + W_1 + W_2 \tag{3.2}$$

where W_0 is the area under the load-deflection curve; $W_1 = P_1\delta_0$, the energy absorbed by the self-

weight of the specimen and δ_0, the deflection when the measured load is zero; and W_2 is the residual energy that needs to fully separate the fractured sample into two halves after the measured load drops to zero, approximately equal to W_1. Therefore, the fracture energy can be calculated by:

$$G_F = \frac{W_0 + 2P_1\delta_0}{A_{lig}} \tag{3.3}$$

where A_{lig} is the fractured area of the sample.

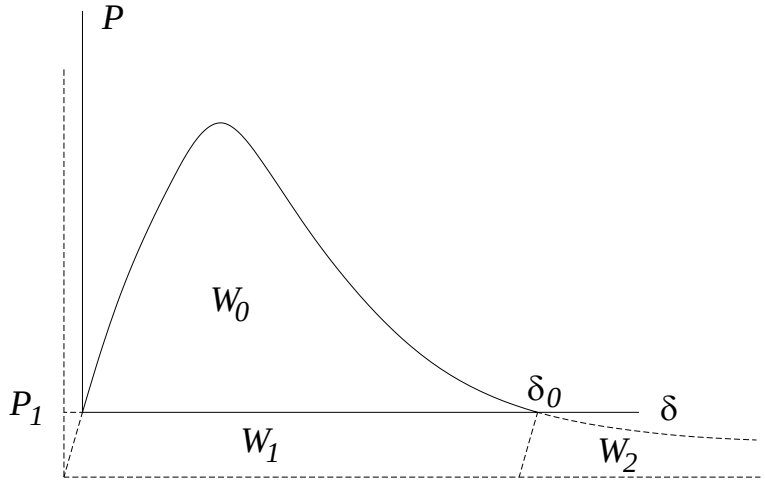

Figure 3.10 Typical load-deflection curve of cohesive fracture test

3.3.3.4 X-ray CT imaging analysis

It has been pointed out that as freeze-thaw conditioning cycles increase, damage accumulation in the form of microcracks in concrete are augmented (Luo et al., 2017). Modulus of elasticity and work energy-based evaluation methods are not capable of revealing microstructural damage in shotcrete under freeze-thaw action, but X-ray computed tomography (CT) with certain resolution is capable of capturing microstructures in shotcrete. The X-ray CT scanning test of conditioned shotcrete samples was conducted at the University of California Irvine (UCI) using the ZEISS Xradia 410 Versa nano-CT (Figure 3.11). Shotcrete samples with

dimensions of 0.956 × 0.956 × 0.956 mm were scanned at 0, 300, and 600 freeze-thaw cycles. With such small samples, the spatial resolution of 2.5 μm (10X) can be achieved to distinguish the heterogeneous microstructure of shotcrete. A single two-dimensional (2D) image was reconstructed from each scanning, and thousands of 2D images at different scanning angles were then collected for each sample and reconstructed to generate a three-dimensional (3D) image using Simpleware ScanIP. Internal damage can be visually detected from 2D images, while heterogeneous spatial distribution of porosity can be characterized from 3D images. Information regarding the pore volume, pore size, and pore distribution can be computed from the final reconstructed 3D images as well.

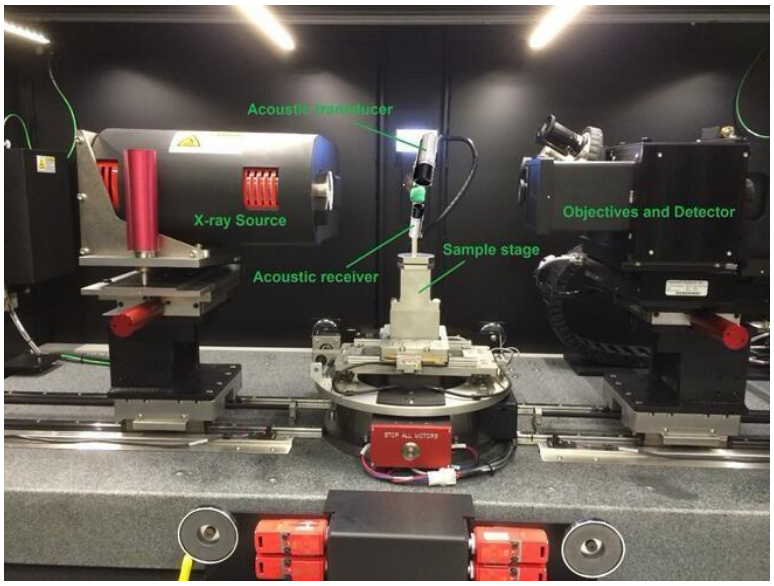

Figure 3.11 Xradia 410 Versa X-ray microscope at UCI

CHAPTER 4. TEST RESULTS AND ANALYSIS

In this chapter, results from the experimental tests conducted on shotcrete specimens are presented and analyzed, with an emphasis on the freeze-thaw durability evaluation of shotcrete.

4.1 Material Properties of Shotcrete

Three rheological properties of freshly mixed shotcrete—slump, air content, and unit weight—were evaluated to achieve a desirable mix design. Afterwards, three basic mechanical properties of the hardened shotcrete of the desirable mix design were evaluated: compressive strength, modulus of elasticity, and flexural strength.

4.1.1 Slump, air content and unit weight

Slump and air content tests were conducted on fresh shotcrete to evaluate its workability and durability properties with adjustment to dosages of high-range water reducing admixture (HRWRA) and air-entraining admixture (AEA). Both the slump test and the air content test for each batch were conducted three times. As illustrated in Table 4.1, the average measured slump for desirable shotcrete was 5.0 inches and the average measured air content for desirable shotcrete was 10.2%. The air content of shotcrete “before shooting” was much higher than the air content of normal concrete, resulting in lower unit weight. This is reasonable because a lot of entrained air is lost after pumping and shooting. Unit weight after shooting increases as well.

Table 4.1 Slump, air content and unit weight of shotcrete

Mixtures	Slump (in.)	Air Content, %	Unit Weight, lb/ft^3
Shotcrete	5.0	10.2	137.7

4.1.2 Compressive strength, modulus of elasticity, and flexural strength

The modulus of elasticity and compressive strength were measured at 7 days, 14 days, and 28 days to study stiffness and strength development with age. The averaged test results of three replicates for the compressive strength and modulus of elasticity are shown in Tables 4.2 along with their variations. It can be seen that the 28-day compressive strength and elastic modulus of the shotcrete mixture used are 6600 psi and 3500 ksi, respectively. Flexural strength or modulus of rupture (MOR) tests on 3 inch × 4 inch × 16 inch prisms were performed at 7 days, 14 days, and 28 days to investigate the tensile strength gain versus time. The averaged testing results for flexural strength are listed in Table 4.2. Shotcrete exhibited a flexural strength of 772 psi at 28 days. Since the addition of silica fume and ground granulated blast-furnace slag (GGBFS), strength gained approximately 70% and 85% of 28-day flexural strength in the early 7 and 14 curing days, respectively.

Table 4.2 Material properties of shotcrete

Age	fc', psi	STDEV	COV	MOE, ksi	STDEV	COV	MOR, psi	STDEV	COV
7	4549	190	4%	2769	73	3%	530	46	9%
14	5354	320	6%	3105	26	1%	588	18	3%
28	6665	220	3%	3501	162	5%	683	12	2%

4.2 Evaluation of Freeze-Thaw Durability

A group of shotcrete beams cast from the same batch was accelerated cured after initial wet curing of 28 days in a freeze-thaw chamber for evaluation of freeze-thaw durability. The measured data, including mass loss and visual inspection of specimen appearance, transverse

frequency, and fracture energy, are given in the following sections. The length change information of specimens is excluded due to lack of measuring equipment.

4.2.1 Surface scaling process and mass loss

The appearance of a typical shotcrete sample at 0, 150, 300, 450, and 600 freeze-thaw cycles is illustrated in Figure 4.1. The mass reduction due to frost action was mainly observed as the scaling of paste and mortar at the bottom surfaces and ends. Surface scaling in the shotcrete became more and more serious as the freeze-thaw cycles increased. Several small pieces of shotcrete at two beam ends spalled after 600 cycles.

(a) 00 cycles

(b) 150 cycles

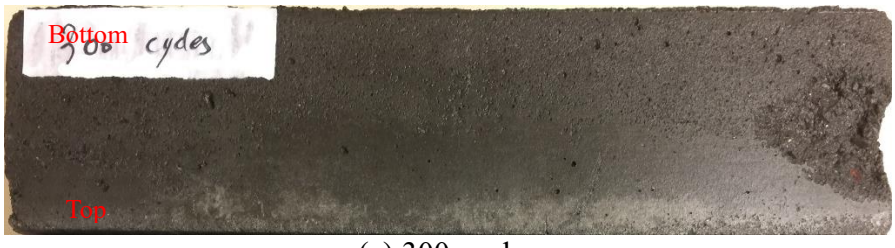

(c) 300 cycles

(d) 450 cycles

(e) 600 cycles

Figure 4.1 Appearance of shotcrete under rapidly repeated freeze-thaw action

Mass reduction of concrete mainly resulted from scaling of paste and small mortar at the bottom surfaces and ends of beams. A comparison of mass loss and loss percentage of shotcrete with respect to freeze-thaw cycles is shown in Figure 4.2. It can be seen from Figure 4.2 that specimen mass keeps decreasing due to accumulative frost action. The mass loss percentages are 1.68% and 2.81% after 300 and 600 freeze-thaw cycles, respectively. Although there is no standard allowable mass loss limit, different levels of mass loss percentage have been assumed in the literature, such as 3%, 5%, and 15% (Kevern et al., 2010). Based on these levels, the shotcrete mixture used in this study was of high durability with the inclusion of silica fume and AEA.

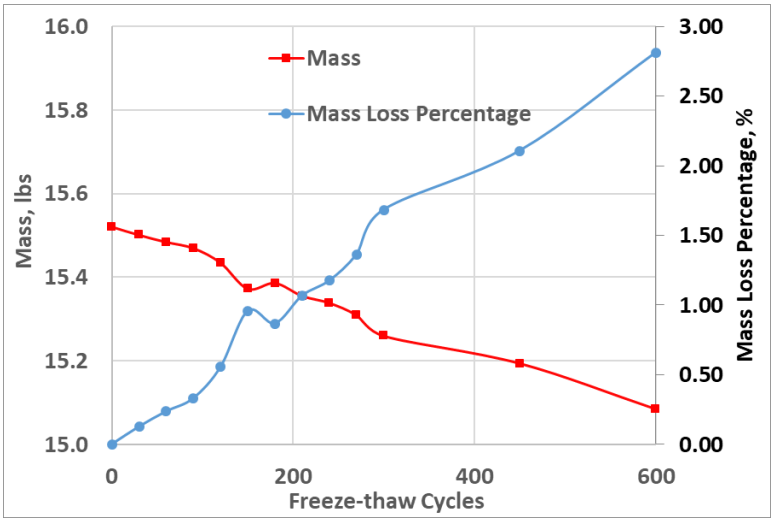

Figure 4.2 Mass loss due to freeze-thaw cycles

4.2.2 Dynamic modulus of elasticity

The nondestructive vibration-based dynamic modulus of elasticity test using an impact hammer was conducted on three shotcrete specimens subjected to rapid freezing and thawing cycles. The natural frequencies from the transverse vibration test were initially measured every 30 freeze-thaw cycles, as depicted in Figure 4.3. Subsequently, the dynamic modulus of elasticity was calculated from the transverse frequencies using Equation 3.1. The dynamic modulus of elasticity and the relative dynamic modulus (RDM) of elasticity with respect to the number of freeze-thaw cycles are comparatively illustrated in Figure 4.4. Due to frost damage, the natural transverse frequency kept decreasing with the increasing number of freeze-thaw cycles. Moreover, the variance of transverse frequency among different samples became more obvious with accumulation of frost damage. Similar to natural frequency, the dynamic modulus of elasticity kept decreasing with the increasing number of freeze-thaw cycles, as depicted in Figure 4.4a. In addition, the variance of the dynamic modulus among different samples became greater. However, according to ASTM C666, the relative dynamic modulus is necessary to characterize material degradation. The relative dynamic modulus of elasticity is calculated as the

ratio of the dynamic modulus at certain freeze-thaw cycles to the initial value of virgin samples. Figure 4.4b shows that the relative dynamic modulus of shotcrete, also defined as the durability factor according to ASTM C666, is 94.15% and 84.33% after 300 and 600 freeze-thaw cycles, respectively. The durability factors are above the ASTM-defined limit (i.e., 60% at 300 freeze-thaw cycles), which implies that no frost failure occurs after more than 600 cycles.

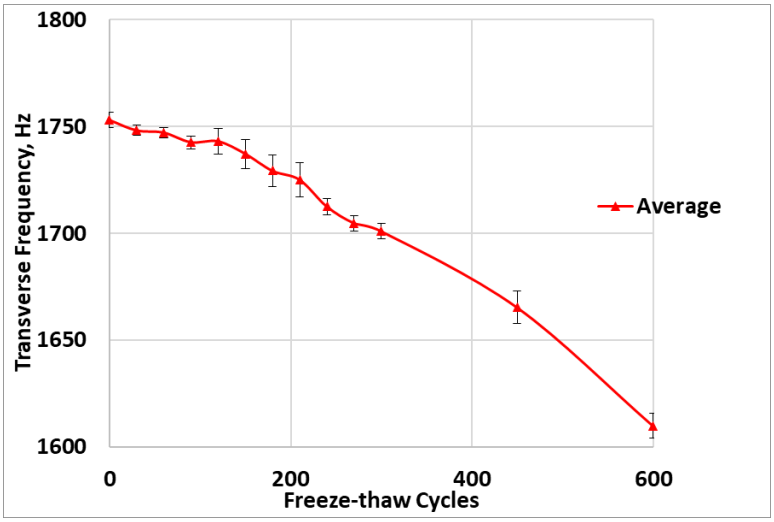

Figure 4.3 Fundamental transverse frequency with respect to freeze-thaw cycles

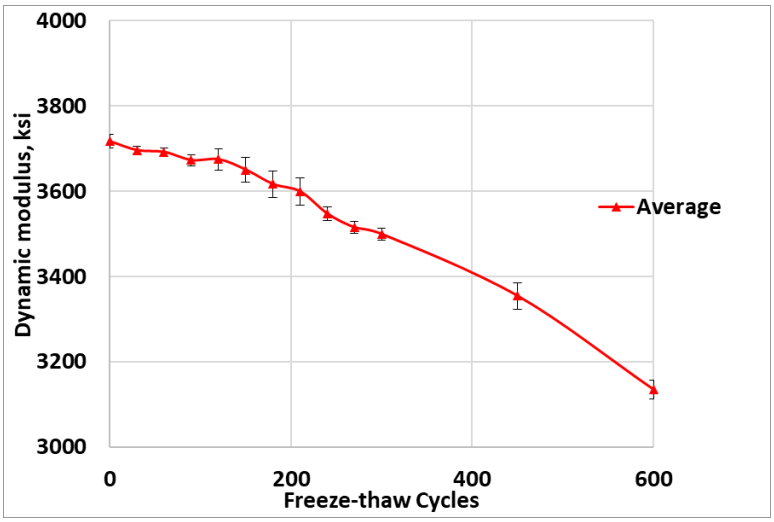

(a) Dynamic modulus

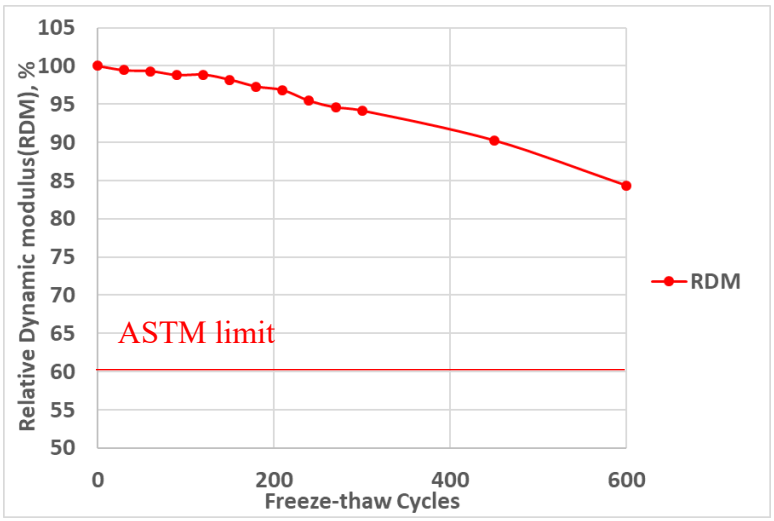

(b) Relative dynamic modulus

Figure 4.4 Dynamic modulus with respect to freeze-thaw cycles

4.2.3 Fracture energy

In parallel with the nondestructive dynamic modulus approach, the cohesive fracture test was conducted on shotcrete beams at different freeze-thaw cycles. More than 24 specimens with dimensions of 3 inch × 4 inch × 16 inch were cast from the same batch and conditioned in the chamber prior to test age. The specimens were perpendicularly notched at the central span and tested at every 60 cycles up to 300 cycles (i.e., 0, 60, 120, 180, 240, 300), and then tested at 450 and 600 cycles. Applied load and mid-span deflection were simultaneously recorded by the machine to obtain the load-deflection (P-δ) curve for each sample. The load-deflection (P-δ) curves for all specimens at a given number of freeze-thaw cycles are plotted in Appendix B, where the applied load is read from the load cell and the mid-span deflection is the average displacement from two LVDTs.

Based on the load-deflection curves, the total absorbed fracture energy values of all samples were calculated using Equations 3.2 and 3.3. The peak loads at fracture and the total fracture energy of shotcrete with respect to the number of freeze-thaw cycles are depicted in

Figures 4.5 and 4.6, respectively. For better comparison of material degradation in terms of peak load and fracture energy, their percentages relative to the virgin (0 cycle or unconditioned) ones are also illustrated. As shown in Figures 4.5 and 4.6, the average flexural peak loads and fracture energy of shotcrete samples kept decreasing due to accumulative freezing and thawing damage. The peak load is only a sole point picked in a load-deflection curve, while the total fracture energy considers the whole fracture work process separating the specimen and is characterized by both ascending and descending branches of the curve. Thus, fracture energy is more representative than peak load in characterizing material degradation. At 300 (ASTM benchmark) freeze-thaw cycles, the relative fracture energy decreasing ratio of shotcrete samples was 83.81% compared with virgin samples. At 600 freeze-thaw cycles, the relative fracture energy decreasing ratio of shotcrete samples was 70.71%, compared with the virgin sample at 0 cycle.

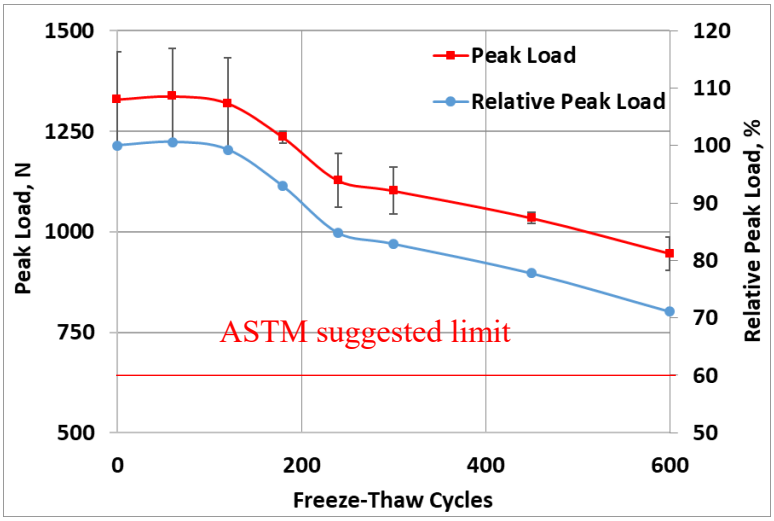

Figure 4.5 Peak load with respect to freeze-thaw cycles

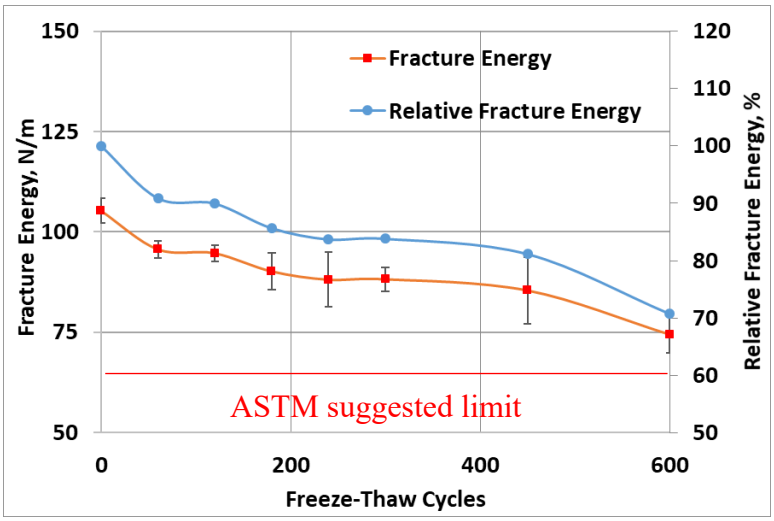

Figure 4.6 Fracture energy with respect to freeze-thaw cycles

4.2.4 Comparison of durability factors

The durability factor can be considered an important parameter in material design to ensure long-term service life. According to ASTM C666, the durability factor refers to the relative dynamic modulus of elasticity at 300 cycles, or the specified number of cycles at which freeze-thaw exposure is terminated. In this study, in comparison with dynamic modulus of elasticity, fracture energy was considered in evaluating the freeze-thaw resistance of shotcrete. Relative fracture energy, as shown in Figure 4.6, is used as a durability factor. The durability factors at either 300 or 600 cycles, as determined from the dynamic modulus and fracture energy tests, are listed in Table 4.3. By comparing the durability factors at either 300 or 600 cycles from two testing approaches, it was found that durability factors based on relative fracture energy are much smaller than those based on relative dynamic modulus, indicating that the fracture energy test is a more sensitive test method than the dynamic modulus of elasticity test for screening damage accumulation caused by frost action and capturing material deterioration when samples are subjected to rapidly repeated freezing and thawing actions as well as other types of cumulative damage. More importantly, fracture energy is associated with the full fracture of

concrete cross section, and thus, it better represents damage or degradation taking place both inside and on/near the surface.

Table 4.3 Comparison of durability factors of different test methods

Cycles	Durability Factor	
	Dynamic Modulus	Fracture Energy
@300	94.15%	83.81%
@600	84.33%	70.71%

4.2.5 X-ray CT scanning analysis

To characterize material degradation due to frost action, internal microstructural damage evolution, porosity, and pore structure were investigated using an X-ray CT scanning machine. Specimens of shotcrete with the dimensions of 0.956 × 0.956 × 0.956 mm were scanned at 0, 300 and 600 freeze-thaw cycles, respectively. Two-dimensional X-ray radiographs were first collected at various viewing angles and then virtually reconstructed to generate a 3D image using Simpleware ScanIP. The reconstructed 3D images can be segmented to separate pores and aggregates from the matrix to obtain porosity and microstructure of shotcrete. Some typical 2D and 3D images of virgin shotcrete at 0 cycle are shown in Figure 4.7. Since the voxel intensity is proportional to the density of the material, it was possible to identify aggregates, matrix, pores, and cracks in the images through the histogram of voxel intensities of each image. Three important features of shotcrete inside can be clearly distinguished after reconstruction: aggregate (gray), cement matrix (dark spots), and air voids (red spots).

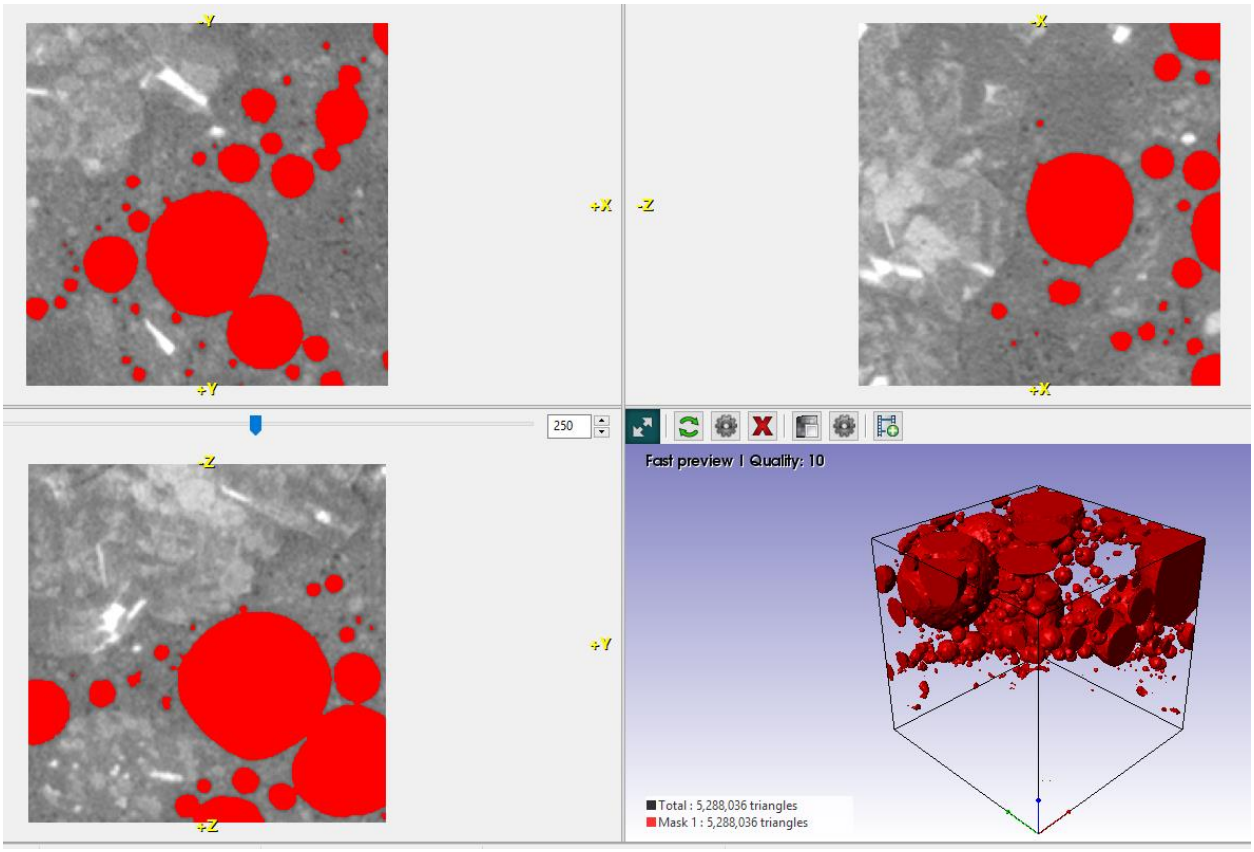

Figure 4.7 2D and 3D reconstructed slices of virgin shotcrete (aggregate, gray; cement matrix, dark spots; air voids, red spots)

A qualitative comparison of one original 2D image of shotcrete was made after each testing cycle to investigate damage evolution in shotcrete due to cyclic freezing and thawing action, as shown in Figure 4.8. Although noises are apparent in these original images, it can still be observed that some information in the images is related to microstructure properties. Some defects and cracks were observed in the aggregate and interface transition zone (ITZ: between aggregate and cement matrix) of conditioned samples. These phenomena became progressively severe and apparent with increasing freezing and thawing action, and they gradually accumulated and grew, resulting in surface scaling and aggregates spalling. The shape of air voids in shotcrete is usually a circle because of the addition of AEA. Discontinuous air voids are shown in Figure 4.8, indicating that air-entrained shotcrete would have enhanced freeze-thaw resistance. The air

voids seem to increase and become larger with the number of freeze-thaw cycles. Choi et al. (2016) stated that pores larger than 1 mm (entrapped air pores) mainly contribute to porosity incensement and are more likely to affect the freeze-thaw resistance of shotcrete. As depicted in Figure 4.8c, at 600 freeze-thaw cycles, the maximum diameter of an air void, 0.7572 mm, is still under this limit. A 0.0175 mm void in such a small sample can even be barely visible to the unaided eye, as very high spatial resolution is conducted. Again, AEA is beneficial in retaining small entrained air bubbles in the matrix and improving the durability of shotcrete.

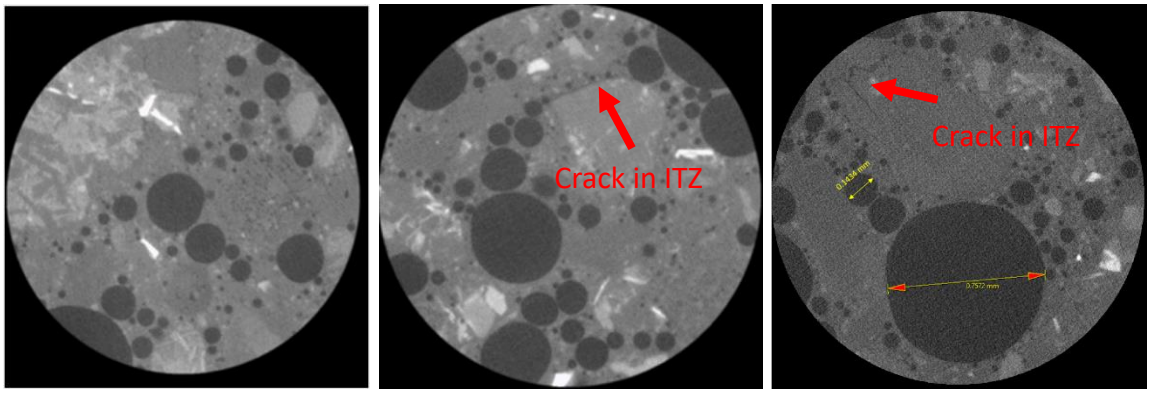

(a) 0 cycles (b) 300 cycles (c) 600 cycles

Figure 4.8 Original 2D images of shotcrete at different freeze-thaw cycles

Three-dimensional imaging analysis and quantitative measurements focusing on the pore structure, e.g., porosity, pore volume, and surface area, were performed on shotcrete at different conditioned cycles. A 3D visualization of the microstructure of shotcrete at 0, 300 and 600 cycles is shown in Figure 4.9. The test data obtained from the reconstructed 3D images are summarized in Table 4.4. The porosity is very high, because the samples scanned consist of a small portion of aggregate, but a large amount of ITZ and air pores. The porosity, pore volume, and surface area correspondingly increased as conditioning action grew. After 300 freeze-thaw cycles, the porosity, pore volume, and surface area increased to 6.6%, 5.6%, 15.6%, respectively. When freezing-thawing reached 600 cycles, the porosity, pore volume, and surface area

increased to 18.8%, 22.2%, 25.8%, respectively. From these increasing ratios compared with virgin samples of 0 cycle, it is noticeable that the deterioration speed of material also increased with the number of freeze-thaw cycles. This is reasonable and expected because defects and cracks formed in previous attacks and provided more channels for moisture diffusion.

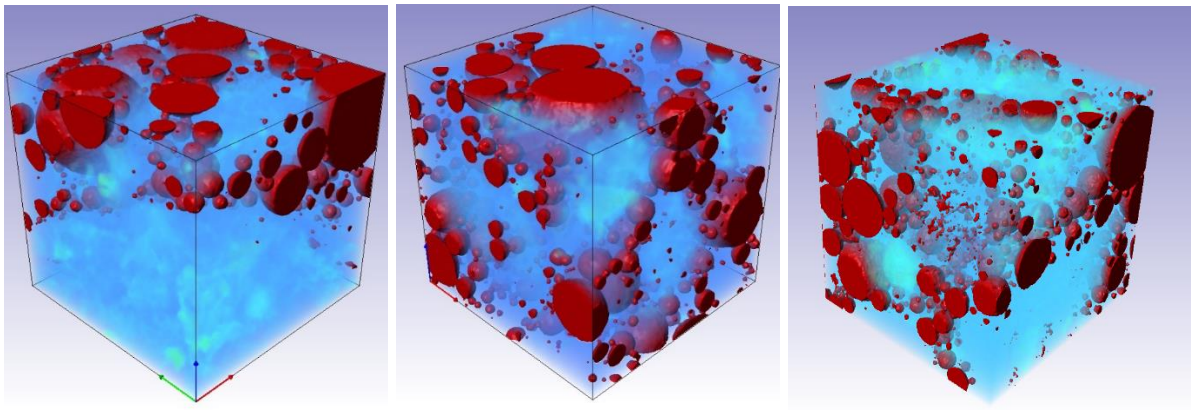

(a) 0 cycles (b) 300 cycles (c) 600 cycles

Figure 4.9 Segmented pores in shotcrete at different freeze-thaw cycles (red: air void system; blue: cement paste and aggregates)

Table 4.4 Pore information in shotcrete

Number of Freeze-Thaw Cycles	Porosity (%)	Pore Volume (mm^3)	Pore Surface Area (mm^2)
0	21.22	0.18	6.71
300	22.63	0.19	7.76
600	25.20	0.22	8.44

4.3 Statistical Damage Analysis

Subjected to rapidly repeated freezing and thawing action, frost damage gradually accumulated in shotcrete over time. The damage evolution due to freeze-thaw attack was characterized using statistical-based probabilistic damage analysis. Eventually, it was feasible to predict the service life of structures at any given damage level.

4.3.1 Statistic regression analysis

The inherent variability in material properties of shotcrete and the related scattering of test data were obvious. Statistical analysis was used initially to build the relation between the number of freeze-thaw cycles and material properties (i.e., relative dynamic modulus and relative fracture energy), so that the remaining service life of structures after certain amounts of time could be predicted. According to the variation of the relative dynamic modulus with respect to freeze-thaw cycles, three-order nonlinear polynomial regression was conducted to build the relationship between the relative dynamic modulus and the freeze-thaw cycles. Similar procedures were also conducted on relative fracture energy.

The regression analysis and scatter plot for relative dynamic modulus with 98% confidence is shown in Figure 4.10(a). Similarly, the regression analysis and scatter plot for relative fracture energy with 95% confidence is shown in Figure 4.10(b). Note that the test data for fracture energy varies more than the test data for dynamic modulus. The regression analysis for relative dynamic modulus (*RDM*) and relative fracture energy (*RFE*) with respect to the number of freeze-thaw cycles (*N*) was established, as expressed in Equations 4.1 and 4.2, respectively. The normal probability plots of the standardized residuals are depicted in Figure 4.11, for both relative dynamic modulus and relative fracture energy. The high value of the adjusted regression coefficient shown in Figure 4.11, $R^2 = 0.995$, indicates that the present three-order nonlinear polynomial prediction models from statistical curve fitting are highly accurate.

$$RDM = 2 \times 10^{-8} N^3 - 4 \times 10^{-5} N^2 - 0.009N + 99.545 \quad (4.1)$$

$$RFE = -4 \times 10^{-7} N^3 + 4 \times 10^{-4} N^2 - 0.136N + 99.911 \quad (4.2)$$

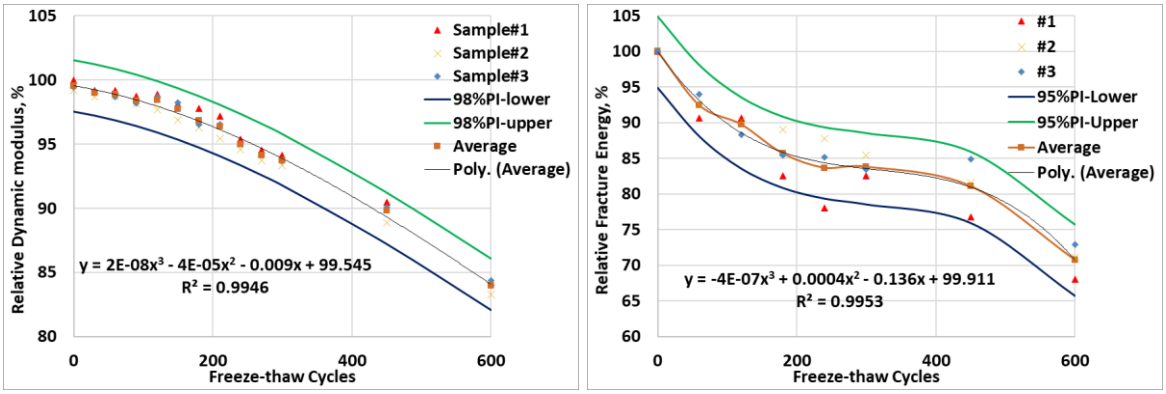

(a) Relative dynamic modulus (b) Relative fracture energy

Figure 4.10 Regression analysis and scatter plot

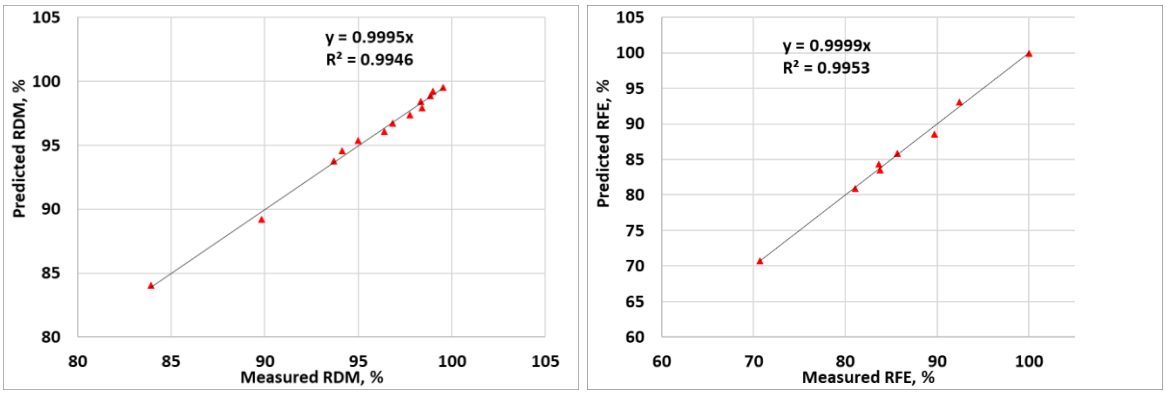

(a) Relative dynamic modulus (b) Relative fracture energy

Figure 4.11 Comparisons of predicted and measured results

4.3.2 Probabilistic damage model

Many researchers have focused on Weibull statistics to predict mechanical properties (such as tensile and compressive strength) and fatigue life of composite materials (Naresh et al., 2018; Zhao and Liu, 2014). The Weibull distribution is more flexible and accurate at predicting strength distribution than other cumulative probability density functions, such as normal distribution. In this study, Weibull statistics were employed to study the variability and reliability of material characterization, which includes dynamic modulus and fracture energy. Moreover, the probability of failure was predicted based on the virgin status (non-damaged) of material properties and under

different prescribed damage levels through probabilistic damage analysis. The fundamental theory for Weibull distribution is briefly discussed as follows.

The three-parameter Weibull distribution was adopted to describe variability in cementitious material characterization at probabilistic damage levels. Freeze-thaw cycles (N) at given cumulative damage levels were assumed to follow the probability density function using a three-parameter Weibull distribution, which can be established as:

$$f(N) = \frac{\beta}{\alpha}\left(\frac{N-\gamma}{\alpha}\right)^{\beta-1} exp\left[-\left(\frac{N-\gamma}{\alpha}\right)^{\beta}\right] \quad (4.3)$$

where α is the scale parameter (characteristic life) that locates the life distribution; $\beta > 0$ is the shape parameter (Weibull modulus) that serves as the inverse measure of the dispersion in freeze-thaw life results; and $\gamma > 0$ is the location parameter, also known as the minimum life parameter.

Integrating probability density function gives the cumulative density function, which is known as the probability of failure and represents the cumulative damage parameter, described as:

$$F(N) = \int_0^N f(s)ds = 1 - exp\left[-\left(\frac{N-\gamma}{\alpha}\right)^{\beta}\right] \quad (4.4)$$

Taking nature logarithms to both sides of Equation (4.4), and then taking further transformation, yield,

$$Y = A + BX \quad (4.5)$$

with $X = \ln(N-\gamma)$, $Y = \ln\left[-\ln\left(1-F(N)\right)\right]$, $A = \beta, and\ B = -\beta ln\alpha$.

Due to the limited number of samples tested, the least square method (LSM) was adopted to determine the statistical parameters in the Weibull model. The cumulative density function in Equation 4.4 is expressed in terms of median rank formula, which is given in Equation 4.6. Based on each set of test data, (X_i, Y_i), coefficients A and B (give α and β) were obtained by applying the linear curve fit, and γ is determined by using the LSM.

$$B(N) = \frac{i-0.3}{n+0.4} \quad (4.6)$$

in which, *i* and *n* are the present and total test numbers in each series, respectively.

The probability of reliability, *R*(*N*), also known as the survival function, of an engineering structure is defined as the probability that the structure remains its own designated state from operating time zero to freeze-thaw life *N*, and it is given as:

$$R(N) = 1 - F(N) = exp\left[-\left(\frac{N-\gamma}{\alpha}\right)^{\beta}\right] \quad (4.7)$$

The failure rate function, *L*(*N*), also known as the hazard function, is the frequency with which an engineering structure fails and is denoted as the number of failures per unit of time. Based on the definition, the failure rate can be mathematically given as

$$L(N) = \frac{f(N)}{R(N)} = \frac{\beta}{\alpha}\left(\frac{N-\gamma}{\alpha}\right)^{\beta-1} \quad (4.8)$$

The accumulated degradation of dynamic modulus and fracture energy versus aging cycles are experimentally determined. Based on one-dimensional continuum damage mechanics, the probabilistic damage variable of shotcrete due to freezing and thawing effects is defined as the ratio of either the dynamic modulus or fracture energy, which can be described as:

$$D = 1 - \frac{E(N)}{E_0} = 1 - RDM(N) \text{ or } D = 1 - \frac{G_F(N)}{G_{F0}} = 1 - RFE(N) \quad (4.9)$$

where $E(N)$ and E_0 are the dynamic modulus of damaged and virgin shotcrete samples, respectively, and $G_F(N)$ and G_{F0} are the fracture energy of damaged and virgin shotcrete samples, respectively. The probabilistic damage variable of shotcrete can be obtained using Eq. (4.4), based on either the dynamic modulus or fracture energy test data.

4.3.3 Probabilistic damage analysis results based on dynamic modulus

Based on test data of the dynamic modulus of shotcrete, the numbers of freeze-thaw cycles needed were obtained for each sample at different damage levels. With respect to the dynamic

modulus, three different damage levels were chosen (i.e., 0.05, 0.10, and 0.15, which corresponds to 95%, 90%, and 85% of the original dynamic modulus). Three obtained freeze-thaw cycles were sorted from smallest to largest (i.e., $N_1 < N_2 < N_3$), as listed in Table 4.4. During the Weibull regression analysis using Equations 4.5 and 4.6, γ was determined by using the LSM, and α and β were obtained from two coefficients A and B of the linear fit, as plotted in Figure 4.12. The corresponding parameters for the Weibull model at different damage levels are summarized in Table 4.5. All correlation coefficients are larger than 0.98, which indicates that the freeze-thaw durability life in terms of dynamic modulus follows the three-parameter Weibull distribution well. From the obtained parameters of the Weibull model, the relation between the probability distribution versus freeze-thaw life cycles for the dynamic modulus at different damage levels was established in terms of the probability density function (PDF) and cumulative distribution function (CDF), as plotted in Figure 4.13.

Table 4.5 Freeze-thaw cycles for relative dynamic modulus at different damage levels

Damage Level (D)	Freeze-Thaw Cycles		
	N_1	N_2	N_3
0.05	226	241	252
0.10	417	453	462
0.15	555	582	584

Table 4.6 Parameters of three-parameter Weibull distribution at different damage levels based on dynamic modulus test

Parameters	Damage (D)		
	0.05	0.10	0.15
α	42.05	92.33	109.76
β	2.50	3.35	6.51
γ	203	358	468
R^2	0.989	0.993	0.983

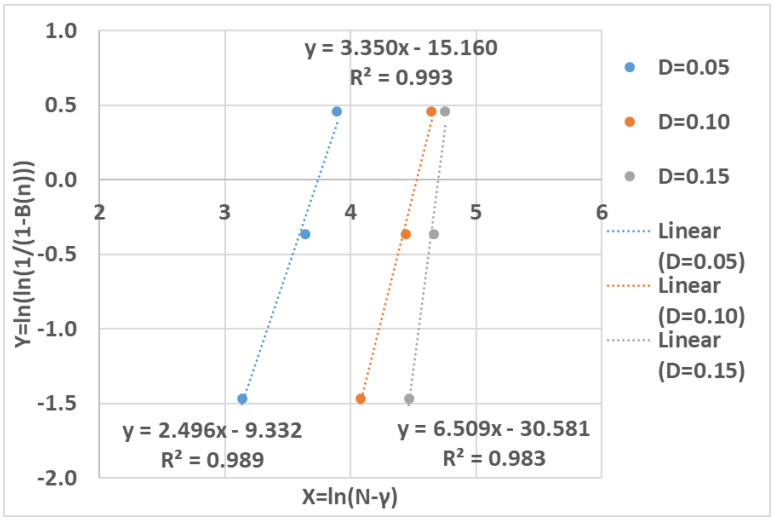

Figure 4.12 Three-parameter Weibull regression results based on dynamic modulus test

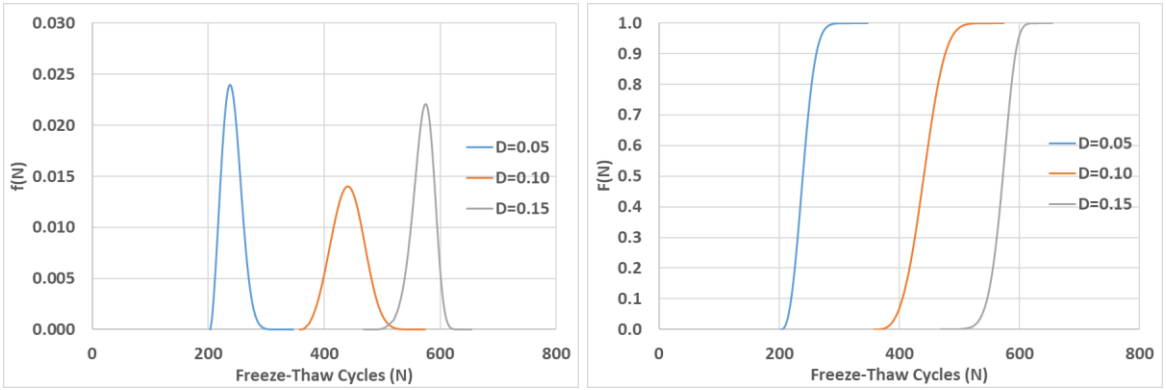

(a) Probability density function (b) Cumulative distribution function

Figure 4.13 Probability distribution of freeze-thaw life cycles based on dynamic modulus test

The reliability function $R(N)$ versus freeze-thaw life cycles of shotcrete at different damage levels is illustrated in Figure 4.14. The reliability function $R(N)$ indicates that the probability of the dynamic modulus remains its own original state under certain freeze-thaw cycles. The variation of the relative dynamic modulus with respect to freeze-thaw cycles is linked by using the reliability function. According to Equation 4.7, since the Weibull distribution is used, the relation between the degradation of dynamic modulus of shotcrete and the number of freeze-thaw cycles exhibits an exponential trend, regardless of the damage level.

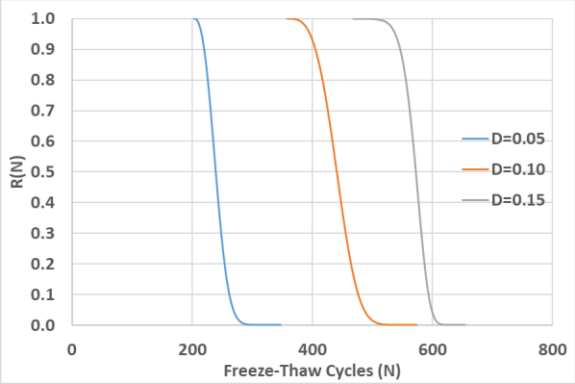

Figure 4.14 Reliability function at different damage levels based on dynamic modulus test

The failure rate function $L(N)$ of shotcrete at different damage levels is illustrated in Figure 4.15, which reveals the failure frequency of structural properties. It can be seen in Figure 4.15 that failure rate increases with the increasing number of freeze-thaw cycles, regardless of damage level. Figure 4.15 also indicates that the potential risk of failure of shotcrete increases as service lifetime grows and freeze-thaw attacks continue. When the freeze-thaw damage reaches higher levels (more freeze-thaw damage accumulates), the failure rate of shotcrete samples increases rapidly, indicating that shotcrete would become less reliable than its original state if it has already accumulated freeze-thaw damage.

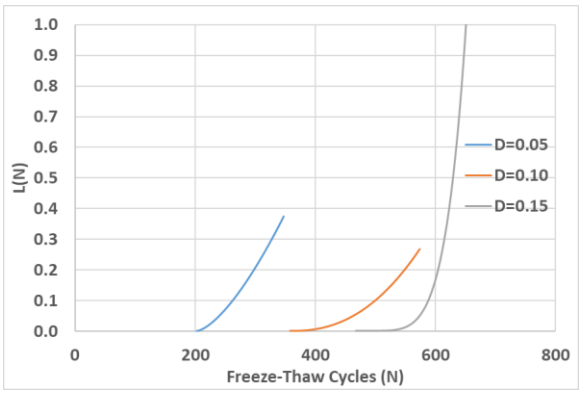

Figure 4.15 Failure rate functions at different damage levels based on dynamic modulus test

From the reliability function of shotcrete under different damage levels, the numbers of freeze-thaw cycles were picked from the curves at corresponding reliability levels, as summarized in Table 4.7. Four different reliability levels were considered: 95%, 90%, 50%, and 10%. A reliability level above 90% is known to mean excellent reliability; below 50% is an unacceptable level. Based on the data in Table 4.7, the relation between the number of freeze-thaw cycles *N* and damage parameter *D* for different reliabilities was accordingly established through three-order polynomial curve fitting, as depicted in Figure 4.16. The analytic fitting formulas of the *N-D* curves for different reliabilities are given in Equations 4.10 to 4.13. As shown in Figure 4.16, all the correlation coefficients R^2 for regression fitting are very close, 1.0, which means that the three-order polynomial model well describes the freeze-thaw cycles *N* at known damage parameters *D* for different reliabilities. In addition, the remaining service life of existing shotcrete structure under freezing and thawing attacks could be determined from the *N-D* relations, if the reliability and damage levels are known. In other words, this proposed probabilistic damage model is competent to predict the service life of existing or newly built shotcrete structures subjected to severe frost damage in cold climates.

$$N = -69333D^3 + 1200D^2 + 5333D \quad \text{at 10\% Reliability} \quad (4.10)$$

$$N = -46667D^3 - 400D^2 + 4917D \quad \text{at 50\% Reliability} \quad (4.11)$$

$$N = -16000D^3 - 4400D^2 + 4660D \quad \text{at 90\% Reliability} \quad (4.12)$$

$$N = 1 \times 10^{-8}D^3 - 7400D^2 + 4690D \quad \text{at 95\% Reliability} \quad (4.13)$$

Table 4.7 Freeze-thaw cycles for different damage levels under different reliabilities based on the dynamic modulus test

Reliability Level	Damage (D)		
	0.05	0.10	0.15
95%	216	395	537
90%	220	406	546
50%	239	441	571
10%	261	476	593

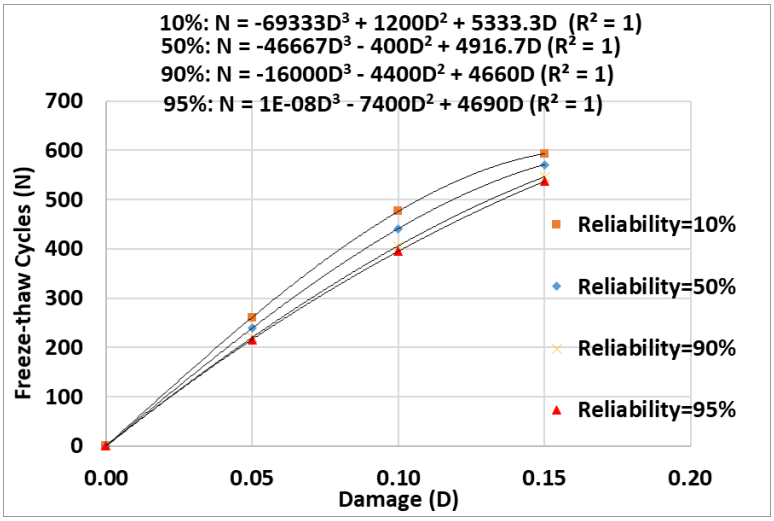

Figure 4.16 Probabilistic relationships between the number of freeze-thaw cycles and damage parameters based on the dynamic modulus test

Another concern is which reliability level predicts service life more accurately. To validate the accuracy of the proposed probabilistic damage model, the experimental data and the predicted results are comparatively plotted in Figure 4.17. It can be seen that the predicted results based on

the polynomial probability model at 50% reliability have the best consistency with the experimental data, indicating that Equation 4.11 provides a more accurate prediction than other equations. The curve plotted from the probability model at 90% reliability shows the trend of lower than the experimental data and thus presents a more conservative and safer prediction.

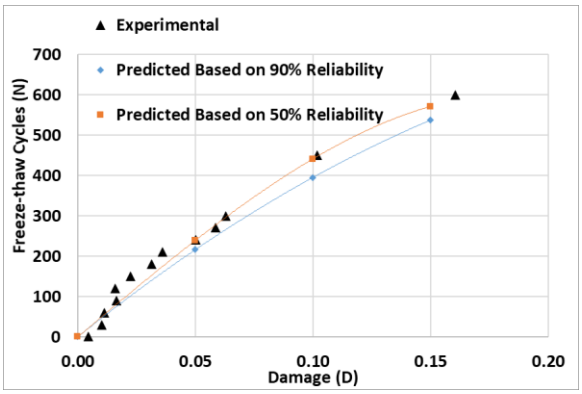

Figure 4.17 Comparison between the predicted and experimental results

4.3.4 Probabilistic damage analysis results based on fracture energy

In similar fashion, the probabilistic damage analysis was conducted using the test data of fracture energy at different freeze-thaw cycles. The number of freeze-thaw cycles of shotcrete with certain damage levels of D = 0.05, 0.10, 0.15, 0.20, and 0.25 are selected from Figure 4.6, corresponding to the relative fracture energy (RFE) of 95%, 90%, 85%, 80%, and 75%, respectively. Three selected freeze-thaw cycles for each damage level were sorted from smallest to largest (i.e., $N_1 < N_2 < N_3$), as summarized in Table 4.8. Then, the same procedure for regression analysis was followed to determine the parameters for the Weibull model at different damage levels, as shown in Figure 4.18. The resulting parameters are summarized in Table 4.9.

Table 4.8 Freeze-thaw cycles for relative fracture energy at different damage levels

Damage Level (D)	Freeze-Thaw Cycles		
	N_1	N_2	N_3
0.05	27	38	48
0.10	99	121	126
0.15	161	246	320
0.20	381	479	520
0.25	482	548	576

Table 4.9 Parameters of three-parameter Weibull distribution at different damage levels based on fracture energy test

Parameters	Damage (D)				
	0.05	0.10	0.15	0.20	0.25
α	36.99	66.14	165.89	211.1	277.46
β	2.86	3.52	1.39	2.06	4.79
γ	5	56	105	280	437
R^2	0.999	0.913	0.983	0.946	0.965

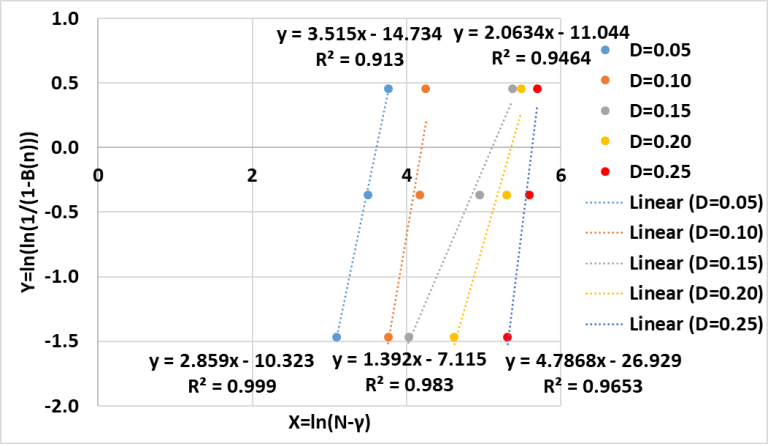

Figure 4.18 Three-parameter Weibull regression results for relative fracture energy

Based on the parameters for the Weibull model, the reliability function $R(N)$ and failure rate function $L(N)$ for shotcrete at different damage levels are shown in Figure 4.19. Figure 4.19a

illustrates the declining trend of shotcrete properties in terms of fracture energy caused by cyclic freeze-thaw conditioning. Similarly, since the Weibull distribution model was used, the relative fracture energy also exhibits exponential decline as freeze-thaw increases. However, as shown in Figure 4.19b, the failure rate of shotcrete in terms of relative fracture energy is different from the failure rate in terms of relative dynamic modulus. That is, as freeze-thaw cycles increase, the failure rate of shotcrete rapidly increases at relatively low damage levels (e.g., D = 0.05, 0.10), but gently increases at relatively high damage levels (e.g., D = 0.15, 0.20, 0.25). At high damage levels, shotcrete becomes more reliable, which is contrary to the conclusion based on the dynamic modulus.

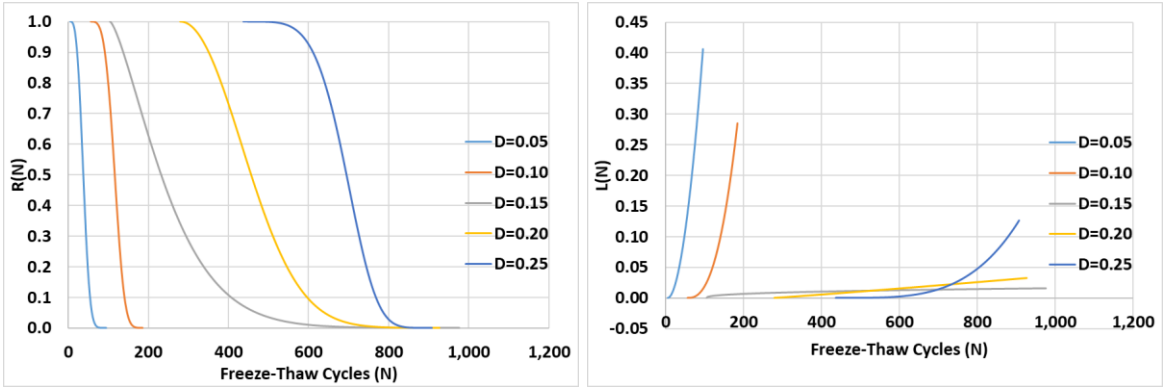

(a) Reliability function (b) Failure rate function

Figure 4.19 Reliability and failure rate functions at different damage levels based on fracture energy test

From the reliability function of shotcrete under different damage levels, the numbers of freeze-thaw cycles were selected from the curves at four reliability levels (i.e., 95 %, 90 %, 50%, 10%), as summarized in Table 4.10. Based on three-order polynomial curve fitting, Equations 4.14 to 4.17 were formed to illustrate the relation between the number of freeze-thaw cycles N and the damage parameter D for different reliabilities. As shown in Figure 4.20, all correlation coefficients R^2 for regression fitting are higher than 0.995, which ensures the accuracy of the three-order

polynomial model. To validate the present model, the predicted data based on the probability model were compared with the experimental data, as shown in Figure 4.21. At the presented damage range (D < 0.25), it was observed that the predicted results based on the polynomial probability model at 50% reliability are more consistent with the experimental results than at 90% reliability, though the model with 90% reliability instills a more conservative and safer prediction.

$$N = -73118D^3 + 34313D^2 - 9345D \quad \text{at 10\% Reliability} \qquad (4.14)$$

$$N = 6452D^3 + 8858D^2 + 180D \quad \text{at 50\% Reliability} \qquad (4.15)$$

$$N = 41245D^3 - 2873D^2 + 597D \quad \text{at 90\% Reliability} \qquad (4.16)$$

$$N = 42799D^3 - 3548D^2 + 571D \quad \text{at 95\% Reliability} \qquad (4.17)$$

Table 4.10 Freeze-thaw cycles for different damage levels under different reliabilities based on fracture energy test

Reliability Level	Damage (D)				
	0.05	0.10	0.15	0.20	0.25
95%	18	84	125	330	586
90%	22	91	138	351	610
50%	38	115	232	457	695
10%	55	140	408	596	768

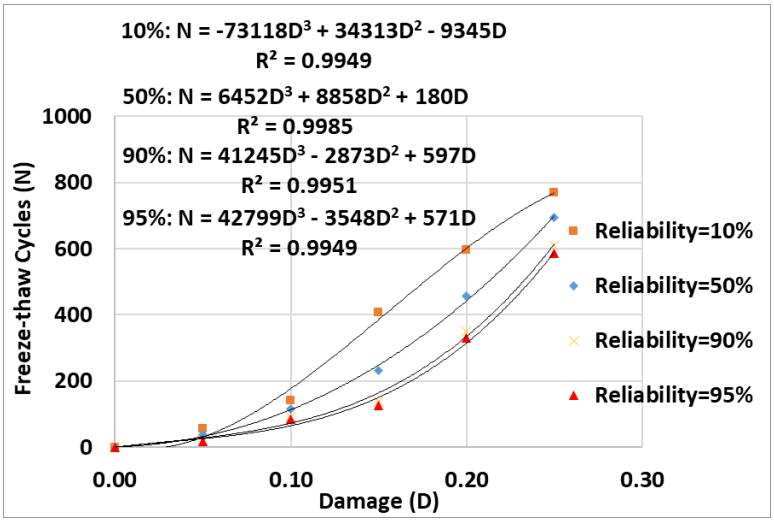

Figure 4.20 Probabilistic relationships between the number of freeze-thaw cycles and damage parameter based on the fracture energy test

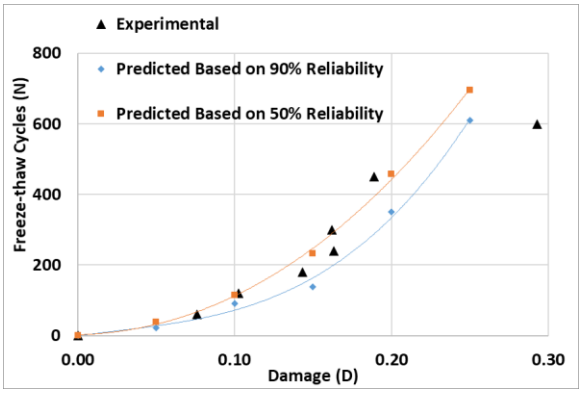

Figure 4.21 Comparison between the predicted and experimental results based on the fracture energy test

CHAPTER 5. CONCLUSIONS AND RECOMMENDATIONS

5.1 Summary

The durability issue of shotcrete has been identified as an important performance aspect for best practices and quality assurance. This study, in conjunction with a related study by the Washington State Department of Transportation (WSDOT) (Qiao and Zhou, 2017), was conducted to investigate the durability and long-term performance of shotcrete in cold climate regions. One selected mixture from the WSDOT was chosen for performance evaluations, including material properties in fresh and hardened states. Long-term freeze-thaw resistance using dynamic modulus of elasticity and fracture energy tests was emphasized. A probabilistic damage analysis was further conducted to establish the relation between the life and the damage parameter for different probabilities of reliability through the three-parameter Weibull distribution model.

5.2 Concluding Remarks

The following are conclusions drawn from the experimental evaluation of the shotcrete mixture.

1. Based on the literature review, long-term durability issues and related evaluation approaches when using shotcrete for structural earth-retaining components were identified. The internal air-void system (air content and spacing factor) of hardened shotcrete significantly influences the durability of shotcrete. Addition of air-entraining admixture results in well-distributed entrained air rather than entrapped air. The freeze-thaw resistance of shotcrete improves with increasing of air content and decreasing of spacing factor. The inclusion of silica

fume in shotcrete mixture generally reduces the mass of scaling residue and improves the durability of shotcrete due to lower permeability.

2. Following the ASTM standard test procedures for concrete and cementitious material characterization, the rheological properties tests (e.g., slump and air content) of freshly mixed shotcrete were conducted to achieve a desirable mix design with acceptable workability (i.e., pumpability and shootability). Adjustment of the amount of air-entraining admixture (AEA) and high-range water reducing admixture (HRWRA) were considered when producing the shotcrete. The average slump and air content for desirable "before shooting" shotcrete are 5 inch and 10.2%, respectively.

3. The long-term freeze-thaw durability of shotcrete was evaluated using standard and non-standard approaches. The rapidly repeated freeze-thaw tests in accordance with ASTM C666 Procedure A were performed on 3 × 4 × 16 inch prisms. The nondestructive method, vibration-based dynamic modulus of elasticity test, was conducted following the ASTM C215 on shotcrete specimens subjected to freeze-thaw conditioning cycles. In parallel, the destructive method, fracture energy test of shotcrete, was conducted by means of the three-point bending test of notched beams. These methods demonstrate that both the dynamic modulus of elasticity and fracture energy tests are capable of determining material deterioration due to accumulative freeze-thaw damage.

4. X-ray CT imaging analysis on conditioned samples is capable of investigating the microstructure of shotcrete, where porosity deterioration can be observed under rapid freeze-thaw attacks. Some defects and cracks were observed in the aggregate, cement matrix, and ITZ of conditioned samples. The deterioration speed of porosity increases with the number of freeze-

thaw cycles because the defects and cracks that have formed in previous attacks provide more channels for moisture diffusion.

5. Mass loss due to frost action was visible as the scaling of paste and mortar at the bottom surfaces and ends. Both the dynamic modulus of elasticity and fracture energy show a decreasing trend with increasing freeze-thaw conditioning cycles. After 300 (ASTM benchmark) freeze-thaw cycles, the relative dynamic modulus of shotcrete was 94.15%; while the fracture energy of shotcrete samples was 83.81%, compared with those corresponding values of virgin samples. The decreasing trends or relative ratios were quite different between the two test methods, i.e., dynamic modulus of elasticity and fracture energy tests. The relative decreasing ratios of fracture energy were much larger than those of dynamic modulus of elasticity. In other words, the durability factors determined from relative fracture energy are much smaller than the durability factors determined from the relative dynamic modulus of elasticity, indicating that the fracture energy test is a more sensitive test method than the dynamic modulus of elasticity test when screening material deterioration over time and capturing cumulative material damage subjected to rapidly repeated freezing and thawing action.

6. The variations of material properties (i.e., dynamic modulus and fracture energy) with respect to freeze-thaw cycles were assessed using the reliability model. The relation between the degradation of dynamic modulus or fracture energy of shotcrete and the number of freeze-thaw cycles exhibits an exponential trend, regardless of the damage level. The failure rate increases as freeze-thaw cycles increase, indicating that shotcrete exhibits more potential risk of failure and is less reliable as service life goes on and freeze-thaw attacks continue. At the studied damage range ($D < 0.25$), it was observed that the predicted results based on the polynomial

probability model at 50% reliability were more consistent with the experimental results than that at 90% reliability, which shows a more conservative and safer prediction.

In summary, to provide best practices of shotcrete for wall fascia and slope stabilization, a desirable shotcrete mixture from WSDOT was tested for its related mechanical properties and evaluation of its durability performance. The fracture energy test method was more sensitive than the dynamic modulus of elasticity test when screening material deterioration/aging effect under freeze-thaw cyclic conditioning. Both prediction results in terms of dynamic modulus and fracture energy demonstrate that the proposed probabilistic damage model is capable of predicting the durability of shotcrete in rapid freezing and thawing action.

5.3 Recommendations

The results of this study are limited to the mix designs and test methods used to explore the proper use of shotcrete. The long-term durability properties of shotcrete are mainly emphasized. Based on the experimental program conducted, the following recommendations are suggested for future study to better understand and improve the durability performance of shotcrete:

1. All specimens with “before shooting” shotcrete are prepared for evaluation and testing of mechanical properties; however, they cannot be identical to those from “after shooting” shotcrete. The comparisons of the mechanical properties and durability of “before shooting” and “after shooting” types of shotcrete should be considered.

2. It is well known that the air-void system in shotcrete significantly influences the mechanical properties and long-term durability performance of shotcrete. In this study, the air content was controlled at 10.2% before shooting, and the air-void system of hardened shotcrete, even after shooting, was still not clear. More laboratory evaluations should be performed to

reveal the effects of air-void characteristics on freeze-thaw durability and to recommend the requirements of air content and spacing factor in shotcrete.

3. X-ray image analysis is capable of determining the air-void characteristics of shotcrete. However, the dimensions of samples scanned in this study are not sufficient/representative to reveal the real porosity. Therefore, more improvements in image analysis of shotcrete are needed in future work.

4. Frost actions were only considered for durability evaluation of shotcrete in this study; however, salty deicers are commonly used in cold regions to melt snow and ice and improve traffic safety. The resistance of shotcrete structures under more severe and combined frost and chemical attacks should be investigated. In addition, possible corrosion of reinforced bars in shotcrete cannot be neglected.

5. Most of the test methods commonly used to characterize shotcrete material properties and performance were adopted from the standard test methods (either ASTM or AASHTO or both) employed for concrete materials. There is a need to develop effective test methods specifically and suitable for characterization of shotcrete. Due to a relative lack of study of shotcrete materials and structures, further studies are needed to systematically develop best curing practices, recommendations for Q/A test methods, and guide specifications for shotcrete in retaining wall fascia and slope stabilization.

REFERENCES

ACI Committee 506R-05. (2005). “Guide to Shotcrete.” American Concrete Institute, Farmington Hills, MI.

ASTM C39-16. (2016). “Standard test method for compressive strength of cylindrical concrete specimens.” ASTM International, West Conshohocken, PA.

ASTM C78-16. (2016). “Standard test method for flexural strength of concrete (using simple beam with third-point loading).” ASTM International, West Conshohocken, PA.

ASTM C127-15. (2015). “Standard Test Method for Relative Density (Specific Gravity) and Absorption of Coarse Aggregate.” ASTM International, West Conshohocken, PA.

ASTM C128-15. (2015). “Standard test method for relative density (specific gravity) and absorption of fine aggregate.” ASTM International, West Conshohocken, PA.

ASTM C136-14. (2014). “Standard Test Method for Sieve Analysis of Fine and Coarse Aggregates.” ASTM International, West Conshohocken, PA.

ASTM C138-16a. (2016). “Standard Test Method for Density (Unit Weight), Yield, and Air Content (Gravimetric) of Concrete.” ASTM International, West Conshohocken, PA.

ASTM C143-15a. (2015). “Standard Test Method for Slump of Hydraulic-Cement Concrete.” ASTM International, West Conshohocken, PA.

ASTM C192-16. (2016). “Standard practice for making and curing concrete test specimens in the laboratory.” ASTM International, West Conshohocken, PA.

ASTM C215-14. (2014). “Standard test method for fundamental transverse, longitudinal, and torsional resonant frequencies of concrete specimens.” ASTM International, West Conshohocken, PA.

ASTM C231-14. (2014). “Standard Test Method for Air Content of Freshly Mixed Concrete by the Pressure Method.” ASTM International, West Conshohocken, PA.

ASTM C457-12. (2012). “Standard Test Method for Microscopical Determination of Parameters of the Air-Void System in Hardened Concrete.” ASTM International, West Conshohocken, PA.

ASTM C469-14. (2014). “Standard test method for static modulus of elasticity and Poisson’s ratio of concrete in compression.” ASTM International, West Conshohocken, PA.

ASTM C666-15. (2015). “Standard test method for resistance of concrete to rapid freezing and thawing.” ASTM International, West Conshohocken, PA.

Banthia, N., Trottier, J. F., and Beaupre, D. (1994). “Steel-Fiber-Reinforced Wet-Mix Shotcrete: Comparisons with Cast Concrete.” *Journal of Materials in Civil Engineering*, 6(3), 430–437.

Bazant, Z. P., Cheran, J. C., Rosenberg, A. M., and Gaidis, J. M. (1988). “Mathematical Model for Freeze-Thaw Durability of Concrete.” *Journal of the American Ceramic Society,* 71(9), 776–783.

Beaupre, D. (1994). “Rheology of High Performance Shotcrete.” Ph.D. Dissertation, the University of British Columbia, Canada.

Beaupre, D., Trottier, J. F., Gendreau, M., et al. (1994). “Deicer Salt Scaling Resistance of Dry- and Wet-Process Shotcrete.” *ACI Materials Journal*, 91(5), 487–494.

Bryne, L. E., Ansell, A., and Holmgren, J. (2014a). “Laboratory testing of early age bond strength of shotcrete on hard rock.” *Tunnelling and Underground Space Technology*, 41, 113–119.

Bryne, L. E., Ansell, A., and Holmgren, J. (2014b). “Investigation of restrained shrinkage cracking in partially fixed shotcrete linings.” *Tunnelling and Underground Space Technology,* 42, 136–143.

Chen, F. L, and Qiao, P. Z. (2015). “Probabilistic damage modeling and service-life prediction of concrete under freeze-thaw action.” *Materials and Structures,* 48(8), 2697–2711.

Chen, J. X., Deng, X. H., Luo, Y. B., He, L. C., Liu, Q., and Qiao X. (2015). “Investigation of microstructural damage in shotcrete under a freeze-thaw environment.” *Construction and Building Materials,* 83, 275–282.

Choi, P., Yeon, J. H., and Yun, K. K. (2016). “Air-void structure, strength, and permeability of wet-mix shotcrete before and after shotcreting operation: The influences of silica fume and air-entraining agent.” *Cement and Concrete Composites,* 70, 69–77.

Choi, S. Y. (2008). “Rheology and Air Void Structures of Wet-mix Shotcrete.” Ph.D. Dissertation, Kangwon National University, Korea.

Crom, T. R. (1981). “Dry-Mix Shotcrete Nozzling.” *Concrete International,* 3(1), 23–26.

Fonseca, P. C., and Scherer, G. W. (2015). “An image analysis procedure to quantify the air void system of mortar and concrete.” *Materials and Structures,* 45, 3087–3098.

Fujiwara, T. (1987). “Deterioration of concrete used in road bridges due to freezing and thawing, Katharine and Bryant Mather International Conference on concrete durability,” *ACI Special Pubication* SP-100, American Concrete Institute, Detroit, MI, 1343–1364.

Heere, R., and Morgan, D. R. (2002). “Determination of Early-Age Compressive Strength of Shotcrete.” *Shotcrete,* Spring, 28–31.

Helmuth, R. A. (1960). “Capillary Size Restrictions on Ice Formation in Hardened Portland

Cement Pastes." Proceedings of the Fourth International Symposium on Chemistry of Cement, Washington, DC., Monograph 43 II Session V Paper VI-S2: 855–869.

Jiang, L., Niu, D. T., Yuan, L. D., and Fei Q. N. (2015). "Durability of concrete under sulfate attack exposed to freeze-thaw cycles." *Cold Regions Science and Technology,* 112, 112–117.

Jolin, M., and Beaupre, D. (2003). "Understanding Wet-Mix Shotcrete: Mix Design, Specifications, and Placement." *Shotcrete*, Summer, 6–12.

Jolin, M., Beaupre, D., Pigeon, M., et al. (1997). "Use of Set Accelerating Admixtures in Dry-Mix Shotcrete." *Journal of Materials in Civil Engineering,* 9(4), 180–184.

Karlsson, L. (1980). "Shotcrete on various rock surfaces." Byggforskningsra det. Report No. R69, in Swedish.

Kevern, J. T., Wang, K. J., and Schaefer, V. R. (2010). "Effect of Coarse Aggregate on the Freeze-Thaw Durability of Pervious Concrete." *Journal of Materials in Civil Engineering*, 22(5), 469–475.

Kim, D. G., Cho, M. S., Lee, J. S., and Lee, H. (2013). "Development of a Prediction Model for Lifespan Reduction Based on the Freezing and Thawing of Cement Paste Composite Material Considering Seasonal Environment." *International Journal of Materials, Mechanics and Manufacturing,* 1(4), 375–378.

Lamontagne, A., Pigeon, M., Pleau, R., and Beaupre, D. (1996). "Use of Air-Entraining Admixtures in Dry-Mix Shotcrete." *ACI Materials Journal,* 93(1), 69–74.

Lee, C. H., Wang, T. T., and Chen, H. J. (2013). "Experimental study of shotcrete and concrete strength development in a hot spring environment." *Tunnelling and Underground Space*

Technology, 38, 390–397.

Luo, Q., Liu, D. X., Qiao, P. Z., Feng, Q. G., and Sun, L. Z. (2017). "Microstructural damage characterization of concrete under freeze-thaw action." *International Journal of Damage Mechanics,* (accepted for publication). https://doi.org/10.1177/1056789517736573

Mainali, G., Dineva, S., and Erling, N. (2015). "Experimental study on debonding of shotcrete with acoustic emission during freezing and thawing cycle." *Cold Regions Science and Technology,* 111, 1–12.

Malmgren, L., Nordlund, E., and Rolund, S. (2005). "Adhesion strength and shrinkage of shotcrete." *Tunnelling and Underground Space Technology,* 20, 33–48.

Morgan D. R. (2003). "Freeze-Thaw Durability of Shotcrete." *Shotcrete,* Spring, 30–37.

Morgan D. R., and Wolsiefer J. (1992). "Wet-Mix Silica Fume Shotcrete: Effect of Silica Fume Form." CANMET/ACI International Conference on Fly Ash, Silica Fume, Slag, and Natural Pozzolans and Natural Pozzolans in Concrete, 1251–1272.

Naresh, K., Shankar, K., and Velmurugan, R. (2018). "Reliability analysis of tensile strengths using Weibull distribution in glass/epoxy and carbon/epoxy composites." *Composites Part B,* 133, 129–144.

Niu, D. T., Wang, Y. D., Ma, R., Wang, J. B., and Xu, S. H. (2015). "Experiment study on the failure mechanism of dry-mix shotcrete under the combined actions of sulfate attack and drying–wetting cycles." *Construction and Building Materials,* 81, 74–80.

Paglia, C., Wombacher, F., and Bohni, H. (2003). "The influence of alkali-free and alkaline shotcrete accelerators within cement systems: Influence of the temperature on the sulfate attack mechanisms and damage." *Cement and Concrete Research,* 33(3), 387–395.

Park, H. G., Suang, S. K., Park, C. G., and Won, J. P. (2008). "Influence of a C12A7 mineral-based accelerator on the strength and durability of shotcrete." *Cement and Concrete Research,* 38, 379–385.

Portland Cement Association. (1998). "Control of Air Content in Concrete." *Concrete Technology Today,* 19(1), 1–3.

Powers, T. C., and Helmuth, R. A. (1953). "Theory of volume changes in hardened Portland cement paste during freezing." *Highway Research Board Proceedings*, 32, 285–297.

Prudencio, L. R. (1998). "Accelerating Admixtures for Shotcrete." *Cement and Concrete Composites,* 20, 213–219.

Qiao, P. Z., and Chen, F. L. (2013). "Cohesive fracture and probabilistic damage analysis of freezing–thawing degradation of concrete." *Construction and Building Materials,* 47, 879–887.

Qiao, P. Z., Mclean, D. I., and Chen, F. L. (2012). "Concrete Performance Using Low-Degradation Aggregates." Research Report No. WA-RD 790.1, Washington State Department of Transportation, Olympia, WA.

Qiao, P. Z., and Zhou, Z. D. (2017). "Best Practices of Using Shotcrete for Wall Fascia and Slope Stabilization (Phase 1 Study)." Research Report No. WA-RD 870.1, Washington State Department of Transportation, Olympia, WA. 102 pages.

RILEM TC-50 FMC. (1985). "Draft Recommendation: Determination of the fracture energy of mortar and concrete by means of the three-point bend tests on notched beams." *Materials and Structures,* 18(106), 285–290.

Sawoszczuk, P., Nokken, M., and Jolin, M. (2013). "Sustainable Shotcrete Using Blast-Furnace

Slag." *Shotcrete,* Fall, 32–37.

Setzer, M. J. (1997). "Action of frost and deicing chemical-basic phenomena and testing. Freeze-thaw durability of concrete." RILEM PROCEEDINGS 30. FREEZE-THAW DURABILITY OF CONCRETE, Edited by Marchand, J., Pigeon, M., and Setzer, M. E&SPON, London, 3–22.

Shen, H., Lin, J., and Mu, E. (2000). "Probabilistic model on stochastic fatigue damage". *International Journal of Fatigue,* 22(7), 569–572.

Sudret, B. (2008). "Probabilistic models for the extent of damage in degrading reinforced concrete structures." *Reliability Engineering & System Safety,* 93(3), 410–422.

Talbot, C., Pigeon, M., Beaupre, D., and Morgan, D. R. (1995). "Influence of Surface Preparation on Long-Term Bonding of Shotcrete." *ACI Materials Journal,* 91(6), 560–566.

U.S. Army Corps of Engineers. (1993). "ENGINEERING AND DESIGN: Standard Practice for Shotcrete." CECW-EG Engineer Manual 1110-2-2005, Washington, DC.

Verma, B. (2015). "Use of Steel Fiber Reinforced Concrete (SFRC) over Plain Concrete for Shotcrete in Underground Tunneling." *SSRG International Journal of Civil Engineering,* 2(7), 9–12.

Wang, J. B., Niu, D. T., Ding, S., Mi, Z. L., and Luo D. M. (2015a). "Microstructure, permeability and mechanical properties of accelerated shotcrete at different curing age." *Construction and Building Materials,* 78, 203–216.

Wang, J. B., Niu, D. T., and Zhang, Y. L. (2015b). "Mechanical properties, permeability and durability of accelerated shotcrete." *Construction and Building Materials,* 95, 312–328.

Won, J. P., Choi, B. R., and Lee, J. W. (2012). “Experimental and statistical analysis of the alkali–silica reaction of accelerating admixtures in shotcrete.” *Construction and Building Materials,* 30, 330–339.

Won, J. P., Hwang, U. J., Kim, C. K., and Lee, S. J. (2013). “Mechanical performance of shotcrete made with a high-strength cement-based mineral accelerator.” *Construction and Building Materials,* 49, 175–183.

Won, J. P., Hwang, U. J., and Lee, S. J. (2015). “Enhanced long-term strength and durability of shotcrete with high-strength C12A7 mineral-based accelerator.” *Cement and Concrete Research,* 75, 121–129.

Yun, K. K., Choi, S. Y., and Yeon, J. H. (2015a). “Correlating rheological properties to the pumpability and shootability of wet-mix shotcrete mixtures.” *Construction and Building Materials,* 98, 884–891.

Yun, K. K., Choi, S. Y., and Yeon, J. H. (2015b). “Effects of admixtures on the rheological properties of high-performance wet-mix shotcrete mixtures.” *Construction and Building Materials,* 78, 194–202.

Zhang, L. J. (2012). “Air Content in Shotcrete: As-Shot Versus As-Batched.” *Shotcrete,* Winter, 50–54.

Zhang, L. J. (2014). “Variability of Compressive Strength of Shotcrete in a Tunnel-Lining Project.” *Shotcrete,* Fall, 22–27.

Zhang, M. H., Mirza, J., and Malhotra, V. M. (1999). “Mechanical Properties and Freezing and Thawing Durability of Polypropylene Fiber-Reinforced Shotcrete Incorporating Silica Fume and High Volumes of Fly Ash.” *Cement, Concrete, and Aggregates,* 21(2), 117–

125.

Zhao, Y. X., and Liu, H. B. (2014). “Weibull modeling of the probabilistic S–N curves for rolling contact fatigue.” *International Journal of Fatigue*,66, 47-54.

APPENDIX

Appendix A: Mix design for shotcrete

Washington State Department of Transportation

Concrete Mix Desig

Contractor	Submitted By	Date
Concrete Supplier	Plant Location	
Contract Number	Contract Name	

This mix is to be used in the following Bid Item No(s): _____

Concrete Class: ***(check one only)***

☐ 3000 ☐ 4000 ☐ 4000D [a] ☐ 4000P [a] ☐ 4000W ☐ Concrete Overlay ☐ Cement Concrete Pavement [d]

■ Other Silica Fume to be added @ 50 lbs/cy

Remarks: _____

Mix Design No. _____ **Plant No.** _____

Cementitious Materials	Source	Type, Class, or Grade	Sp. Gr.	Lbs/cy
Cement	Ssangyong Cement	Type I-II	3.15	705
Fly Ash [a]				
GGBFS	Lafarge Cement	Grade 100	2.4	40
Latex				
Microsilica	Force 10000	Dry Silica Fume	2.20	50

Concrete Admixtures	Manufacturer	Product	Type	Est. Range (oz/cy)
Air Entrainment	W.R. Grace	Daravair 1000		0.1 - 25 oz/cwt
Water Reducer				
High-Range Water Reducer	W.R. Grace	ADVA 195	F-HRWR(min 12%)	0.1 - 30 oz/cwt
Set Retarder				
Other				

Water (Maximum) 267 (lbs/cy) Is any of the water Recycled or Reclaimed? Yes[e] ☐ No ■

Water/Cementitious Ratio (Maximum) 0.34 Mix Design Density: 146.83 lbs/cf[d]

Design Performance	1	2	3	4	5	Average[f]
28 Day Compressive Strength (cylinders) psi	6963	8543	6123	7780	7720	7,426
14 Day Flexural [d] Strength (beams) psi						-

Agency use only: Check appropriate box

☐ This mix design **Meets Contract Specifications** and may be used on the bid items noted above.

☐ This mix design **Does Not Meet Contract Specifications** and is being returned for corrections.

Reviewed By: _____ (PE Signature) _____ (Date)

DOT Form 350-040 EF Revised 6/06

Distribution: Original - Contractor
Copies To - State Materials Lab-General Materials Eng. ; Regional Materials Lab; Project Inspector

Figure A.1 Mix design of shotcrete

Combined Gradation Chart

Concrete Aggregates	Component 1	Component 2	Component 3	Component 4	Component 5	Combined Gradation
WSDOT Pit No.	PS-X-125	PS-X-125				
WSDOT ASR 14-Day Results (%)[b]	☐ Yes ☐ No	☐ Yes ☐ No	☐ Yes ☐ No	☐ Yes ☐ No	☐ Yes ☐ No	
Grading [c]	WSDOT Class 2 BLD_SAND	AASHTO #8 AGG_3/8				
Percent of Total Aggregate	73	27				100%
Specific Gracvity	2.69	2.74				
Lbs/cy (ssd)	2120	790				

Percent Passing

2 inch	100.0	100.0	-	-	-	100.0
1-1/2 inch	100.0	100.0	-	-	-	100.0
1 inch	100.0	100.0	-	-	-	100.0
3/4 inch	100.0	100.0	-	-	-	100.0
1/2 inch	100.0	100.0	-	-	-	100.0
3/8 inch	100.0	87.0	-	-	-	96.5
No. 4	100.0	20.0	-	-	-	78.3
No. 8	92.0	1.0	-	-	-	67.3
No. 16	68.0	-	-	-	-	49.5
No. 30	43.0	-	-	-	-	31.3
No. 50	13.0	-	-	-	-	9.5
No. 100	3.0	-	-	-	-	2.2
No. 200	0.9	-	-	-	-	0.7

Fineness Modulus: 2.86 (Required for Class 2 Sand)

ASR Mitigation Method Proposed[b]: _____

Notes:

a Required for Class 4000D and 4000P mixes.

b Alkali Silica Reactivity Mitigation is required for sources with expansions over 0.20% - Incidate method for ASR mitigation.
For expansion of 0.21% - o.45%, acceptable mitigation can be the use of low alkali cement or 25% type F fly ash.
Any other proposed mitigation method or for pits with greater than 0.45% expansion, proof of mitigating measure, either ASTM C1260 / AASHTO T303 test results must be attached.
If ASTM C 1293 testing has been submitted indicating 1-year expansion of 0.04% or less, mitigation is not required.

c AASHTO No. 467, 57, 67, 7, 8; WSDOT Class 1, Class 2; or combined gradation. See Standard Specification 9-03.1.

d Required for Cement Concrete Pavements.

e Attach test results indicating conformance to Standard Specification 9-25.1.

f Actual Average Strength as determined from testing or estimated from ACI 211.

DOT Form 350-040 EF
Revised 6/06

Figure A.2 Combined gradation of aggregates

Appendix B: Load-deflection curves from cohesive fracture tests

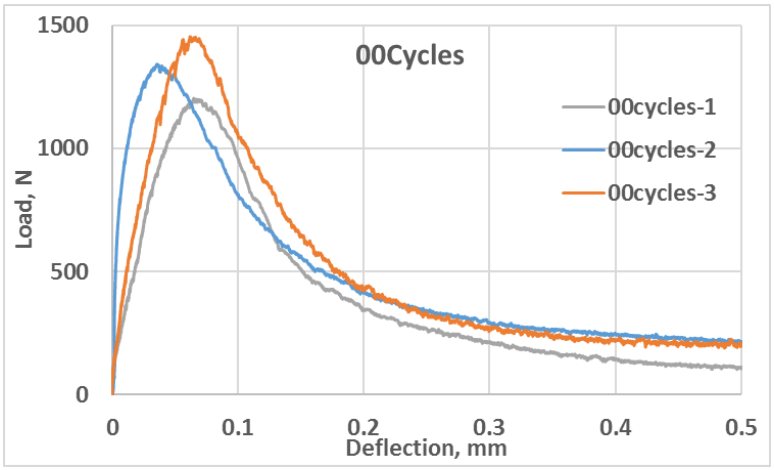

(a) 0 cycles

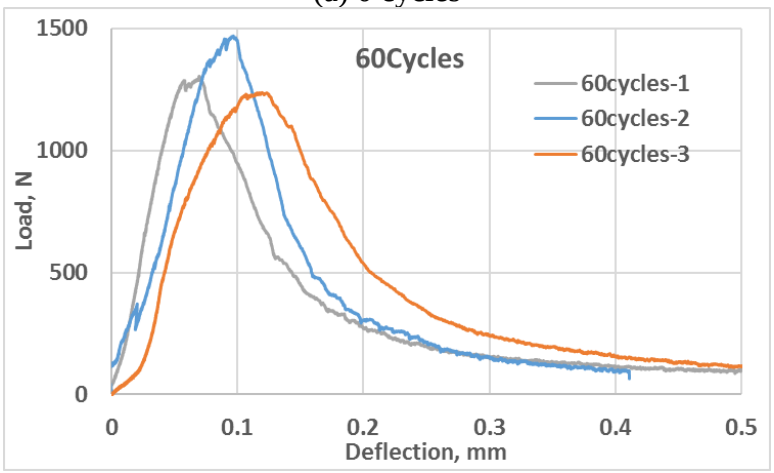

(b) 60 cycles

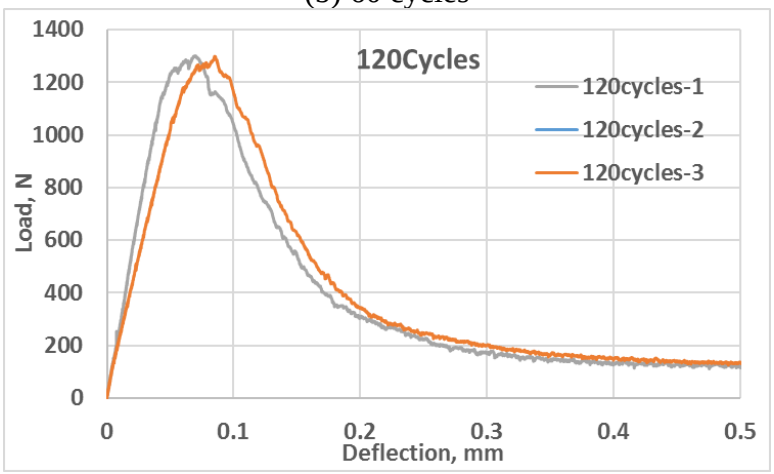

(c) 120 cycles

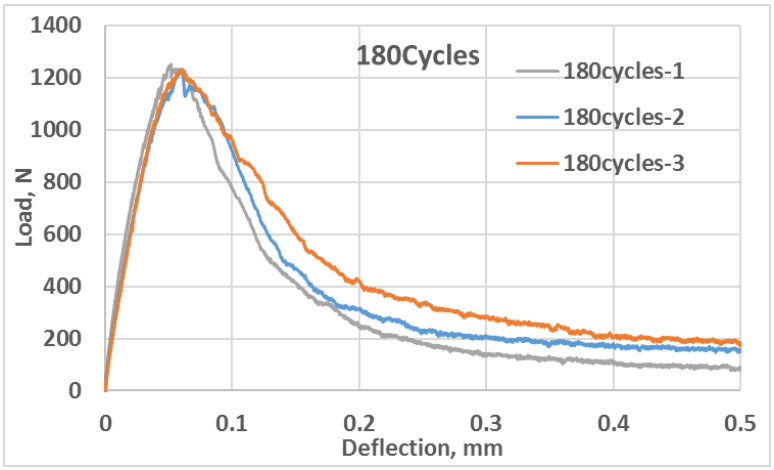

(d) 180 cycles

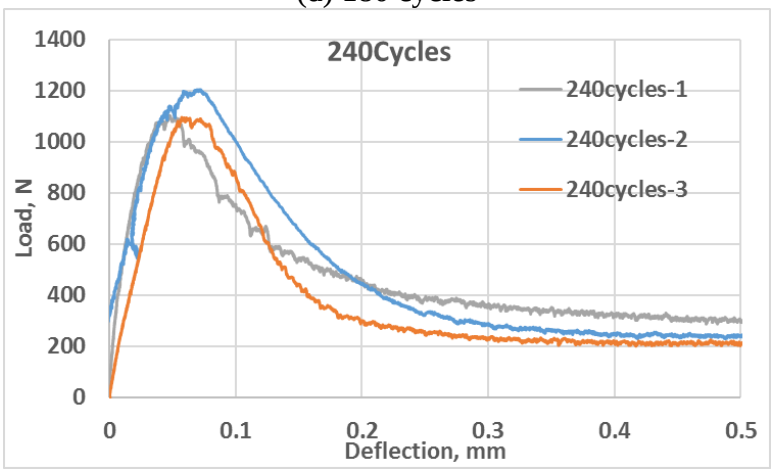

(e) 240 cycles

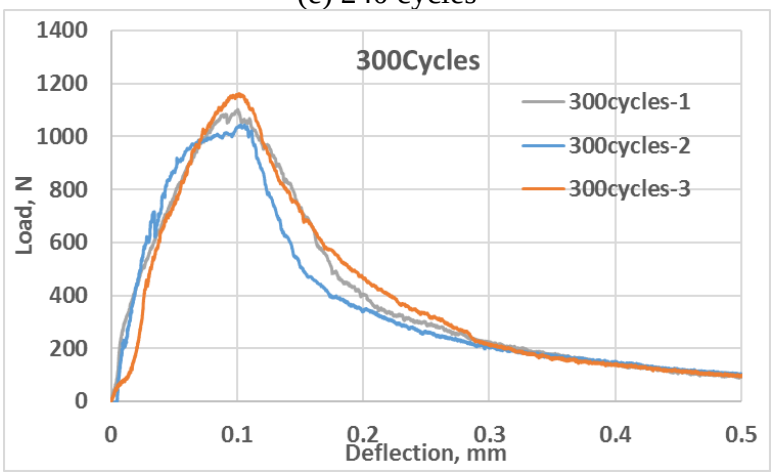

(f) 300 cycles

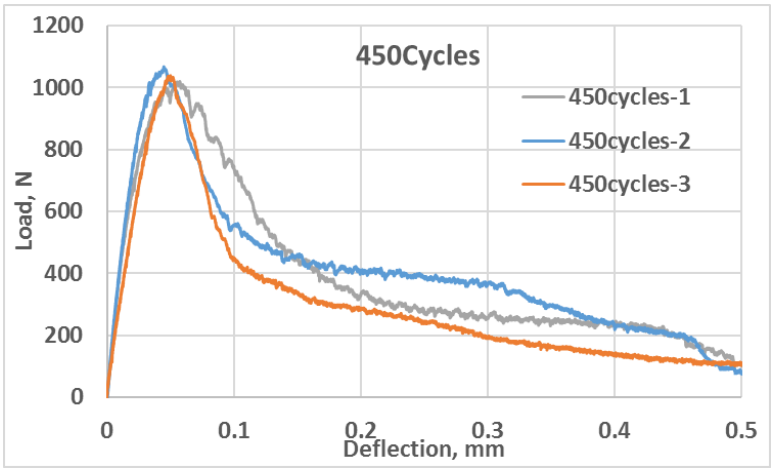

(g) 450 cycles

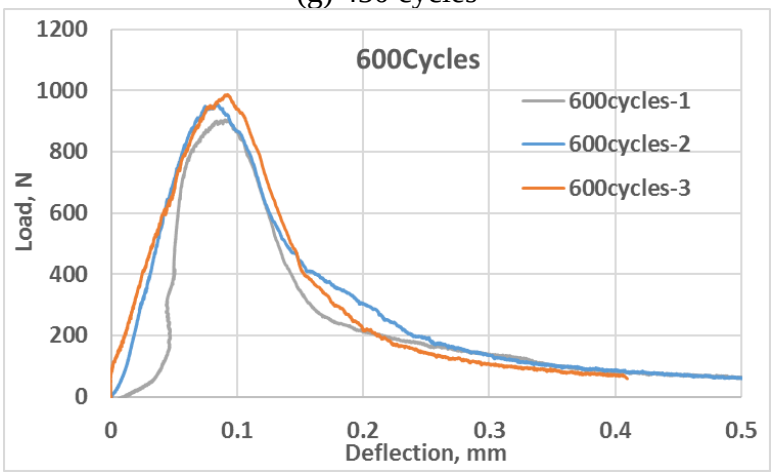

(h) 600 cycles

Figure B.3 Load-deflection curves of shotcrete at different freeze-thaw cycles